PERGAMON

International Journal of Solids and Structures 37 (2000) 6635–6682

INTERNATIONAL JOURNAL OF SOLIDS and STRUCTURES

www.elsevier.com/locate/ijsolstr

Kinked crack in anisotropic bodies

S. Yang, F.-G. Yuan*

Department of Mechanical and Aerospace Engineering, North Carolina State University, Box 7910, Raleigh NC 27695, USA

Received 27 October 1998; received in revised form 21 July 1999

Abstract

Solutions are presented for a crack kinking out of the crack plane in a generally anisotropic elastic body under two-dimensional deformation. Based on Stroh formalism, a system of singular integral equations governing the kinking crack with small kink length is given in a simple, straightforward form. The explicit expressions of the stress intensity factors, *T*-stresses, and energy release rates at the kinked crack tip are presented in terms of some nondimensional coefficients together with the stress intensity factors, *T*-stresses, and the coefficients of the third term acting on the main crack tip prior to crack kinking. The nondimensional coefficients depend on kink angle and material constants, but not on kink length. The energy release rate ratio which may characterize the competition along different crack growth directions is provided. The role of *T*-stresses and the third-term applied at the main crack field are determined which can be significant in the kinking and the stability of the kinked crack. Based on the energy release rate fracture criterion, the stability condition of the kinked crack is derived. The influences of anisotropy and loading mixity on the implications of crack kinking behavior is also given. The results for monoclinic materials with symmetry plane at $x_3 = 0$ are derived from general results. Numerical results for the stress intensity factors, *T*-stresses at the kinked acrack tip and the energy release rate ratio for some special cases are provided. The dimensionless coefficients for crack kinking of orthotropic materials at the right angle to the main crack plane are tabulated.

Keywords: Crack kinking; Anisotropic materials; Stress intensity factor; Energy release rate; *T*-stress; *g*-term; Fracture criterion; Singular integral equations; Stability of kinked crack

1. Introduction

The direction of crack kinking can be one of the major factors in determining the residual strength of the structural components. Therefore, proper prediction of the kinked direction upon crack initiation and growth is of great importance in structural analysis. In order to assess whether the crack will extend in the crack plane or advance by kinking out of the crack plane, the stress field near the kink tip and

* Corresponding author. Fax: +1-919-515-5934.

0020-7683/00/$ - see front matter
PII: S0020-7683(99)00222-X

associated fracture parameters need to be quantified. Crack kinking analyses for isotropic materials have been extensively carried out. Khrapkov (1971, 1998), Bibly and Cardew (1975) and Melin (1994), etc. used the Mellin transform to obtain the stress intensity factors in front of the kinked tip for infinitesimal kink. Using Muskhelishvili's complex stress functions and perturbation methods, Banichuk (1970), Gol'dstein and Salganik (1974), Cotterell and Rice (1980), etc. determined the stress intensity factors for small kinked angle and infinitesimal kinks. Cotterell and Rice (1980) also considered the effect of the T-stress on the kinked stress intensity factors. Sumi et al. (1983) utilizing the perturbation technique and an alternating method developed a solution for a finite geometry. Lo (1978), Hayashi and Nemat-Nasser (1981), He and Hutchinson (1989) and He et al. (1991) calculated the stress intensity factors by the use of singular integral methods with dislocations and identified the role of T-stress on the kinking behavior in isotropic materials.

For anisotropic materials using Lekhnitskii's formalism and dislocation technique, Miller and Stock (1989) formulated the kinking problem in generally anisotropic materials using Lekhnitskii's complex potential and calculated stress intensity factors for orthotropic materials under remote tension loading. Obata et al. (1989) analyzed in-plane deformation and calculated stress intensity factors and energy release rate at the kinked crack tip due to stress intensity factors of the main crack for orthotropic materials, and Selvarathninam (1995) analyzed the crack kink behavior under uniform loading at infinity in orthotropic materials. Gao and Chiu (1992) using the Stroh formalism obtained the perturbation solution for infinitesimal kink and small kink angle under in-plane deformation. Suo et al. (1991) obtained the stress intensity factors for orthotropic materials with kink angle normal to the crack plane.

In this paper, the Stroh formalism of anisotropic elasticity combined with singular integral equation approach are used to determine the stress intensity factors and energy release rate for arbitrary kink angles including the effects of T-stress and the third-term. The stability condition of the kinked crack is derived from the energy release rate fracture criterion. The T-stresses for the kinked crack in terms of stress intensity factors and T-stresses prior to thinking are also formulated.

2. General formulation for kinked crack tip field

The attention focuses on a kinked crack in an anisotropic elastic body under two-dimensional deformation. Referring a fixed coordinate system x_1, x_2, x_3, the strain–stress law is

$$\boldsymbol{\varepsilon} = \boldsymbol{s}'\boldsymbol{\sigma} \tag{2.1}$$

where

$$\boldsymbol{\varepsilon} = [\varepsilon_1, \varepsilon_2, \gamma_{23}, \gamma_{31}, \gamma_{12}]^{\mathrm{T}}, \qquad \boldsymbol{\sigma} = [\sigma_{11}, \sigma_{22}, \sigma_{23}, \sigma_{31}, \sigma_{12}]^{\mathrm{T}}$$

$\boldsymbol{s}' = [s'_{ij}]$ are reduced compliance coefficients defined by $s'_{ij} = s_{ij} - s_{i3}s_{j3}/s_{33}$, $(i, j, = 1, 2, 4, 5, 6)$.

Consider a crack with kink segment of length a kinking out of the crack plane at an angle ω in a linear anisotropic body as shown in Fig. 1. When a is small compared with all in-plane geometric lengths, including the length of the main crack, the parent crack is taken as semi-infinite and stresses remotely asymptote to

$$\sigma_{\alpha\beta} = \sum_{i=1}^{3} \frac{k_i}{\sqrt{2\pi r}} \sigma^i_{\alpha\beta}(\theta; s'_{ij}) + T_1\delta_{\alpha 1}\delta_{\beta 1} + T_3\delta_{\alpha 3}\delta_{\beta 1} + \sum_{i=1}^{3} \sqrt{\frac{2r}{\pi}} g_i \tau^i_{\alpha\beta}(\theta; s'_{ij}) + O(r^1), \quad \sigma_{\alpha\beta} \neq \sigma_{33} \tag{2.2}$$

where r and θ are the cylindrical coordinate centered at the main crack tip; $\boldsymbol{k} = [k_2, k_1, k_3]^{\mathrm{T}}$,

$\boldsymbol{T} = [T_1, 0, T_3]^{\mathrm{T}}$, $\boldsymbol{g} = [g_2, g_1, g_3]^{\mathrm{T}}$ are stress intensity factors, T-stresses and real coefficients of the third term (g-term) acting the main crack tip for $a = 0$. The T-stress terms, T_1 and T_3, are constant stress terms for σ_{11} and σ_{13} prior to kinking. $\sigma^i_{\alpha\beta}$ and $\tau^i_{\alpha\beta}$ depend on θ and s'_{ij}; $\boldsymbol{T}$ and $\boldsymbol{g}$ depend on s'_{ij}, loading, and geometry. In other words, for small a, the actual geometry of the cracked body and the applied loads can be represented by the remote loading $\boldsymbol{k}$, $\boldsymbol{T}$, $\boldsymbol{g}$, etc.. Here, $\boldsymbol{k}$, $\boldsymbol{T}$ and $\boldsymbol{g}$ are known which have been determined from the actual body geometry and loading (see Yang and Yuan, 1999). In what follows, attention is focused on the case where the crack surfaces are traction free under remote loading $\boldsymbol{k}$, $\boldsymbol{T}$ and $\boldsymbol{g}$. The stress field at the tip of the kinked crack is the classical field with conventional stress intensity factors, $\boldsymbol{k}' = [k'_2, k'_1, k'_3]^{\mathrm{T}}$ and T-stresses, $\boldsymbol{T}' = [T'_1, 0, T'_3]^{\mathrm{T}}$. Based on the linearity and dimensional consideration, it can be shown that for small a, $\boldsymbol{k}'$ and $\boldsymbol{T}'$ are related to the factors $\boldsymbol{k}$, $\boldsymbol{T}$, and $\boldsymbol{g}$ applied at the parent crack tip when $a = 0$ by

$$\begin{bmatrix} k'_2 \\ k'_1 \\ k'_3 \end{bmatrix} = \begin{bmatrix} c_{22} & c_{21} & c_{23} \\ c_{12} & c_{11} & c_{13} \\ c_{32} & c_{31} & c_{33} \end{bmatrix} \begin{bmatrix} k_2 \\ k_1 \\ k_3 \end{bmatrix} + \sqrt{a} T_1 \begin{bmatrix} b_{21} \\ b_{11} \\ b_{31} \end{bmatrix} + \sqrt{a} T_3 \begin{bmatrix} b_{23} \\ b_{13} \\ b_{33} \end{bmatrix} + a \begin{bmatrix} h_{22} & h_{21} & h_{23} \\ h_{12} & h_{11} & h_{13} \\ h_{32} & h_{31} & h_{33} \end{bmatrix} \begin{bmatrix} g_2 \\ g_1 \\ g_3 \end{bmatrix} + O(a^{3/2}) \tag{2.3}$$

$$\begin{bmatrix} T'_1 \\ T'_3 \end{bmatrix} = \frac{1}{\sqrt{a}} \begin{bmatrix} d_{12} & d_{11} & d_{13} \\ d_{32} & d_{31} & d_{33} \end{bmatrix} \begin{bmatrix} k_2 \\ k_1 \\ k_3 \end{bmatrix} + \begin{bmatrix} e_{11} & e_{13} \\ e_{31} & e_{33} \end{bmatrix} \begin{bmatrix} T_1 \\ T_3 \end{bmatrix} + O(\sqrt{a}) \tag{2.4}$$

where the coefficients, c_{ij}, b_{ij}, h_{ij}, d_{ij}, and e_{ij}, are functions of ω and s'_{ij}, O represents the other higher-order terms.

The above expressions of $\boldsymbol{k}'$ and $\boldsymbol{T}'$ can be derived from a system of integral equations governing the kinked crack-tip field and the values of c_{ij}, b_{ij}, h_{ij}, d_{ij}, and e_{ij} can be calculated by solving the integral

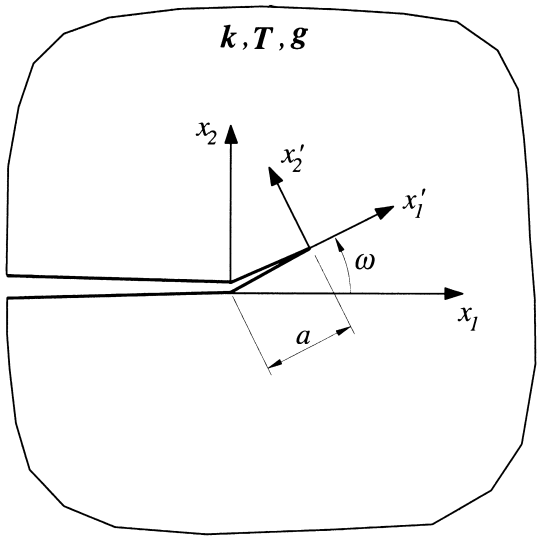

Fig. 1. A kinked crack with length a emanating from the main crack with angle ω.

equations (see later sections). For a monoclinic material with the symmetry plane at $x_3 = 0$, the in-plane deformation is separated from the anti-plane deformation. Therefore, Eqs. (2.3) and (2.4) become:

For in-plane deformation,

$$\begin{bmatrix} k_2' \\ k_1' \end{bmatrix} = \begin{bmatrix} c_{22} & c_{21} \\ c_{12} & c_{11} \end{bmatrix} \begin{bmatrix} k_2 \\ k_1 \end{bmatrix} + \sqrt{a} T_1 \begin{bmatrix} b_{21} \\ b_{11} \end{bmatrix} + a \begin{bmatrix} h_{22} & h_{21} \\ h_{12} & h_{11} \end{bmatrix} \begin{bmatrix} g_2 \\ g_1 \end{bmatrix}$$

$$T_1' = (d_{12} k_2 + d_{11} k_1)/\sqrt{a} + e_{11} T_1 \tag{2.5}$$

For anti-plane deformation,

$$k_3' = c_{33} k_3 + \sqrt{a} T_3 b_{33} + a h_{33} g_3$$

$$T_3' = d_{33} k_3/\sqrt{a} + e_{33} T_3 \tag{2.6}$$

For in-plane deformation in isotropic materials, the values of c_{ij} and b_{i1} can be calculated using an integral equation method described by He and Hutchinson (1989). For the isotropic case, c_{ij} and b_{i1} depend on ω only, the values of c_{ij} are given by Hayashi and Nemat-Nasser (1981), He and Hutchinson (1989) and Melin (1994), b_{i1} by He et al. (1991). For in-plane deformation in anisotropic solids, Miller and Stock (1989) and Obata et al. (1989) calculated c_{ij}. For orthotropic solids, $c_{ij}(\omega = -\pi/2; s_{ij}')$ are given by Suo et al. (1991).

In this paper, the Stroh formalism of anisotropic elasticity combined with integral equation approach are used to determine the stress intensity factors for arbitrary kink angles including the effects of T-stresses and g-term on the stress intensity factors. As a first step, a system of integral equations governing the kinked crack problem is constructed using a basic solution for a line dislocation interacting with a semi-infinite crack. The basic solution may be obtained by superimposing the following two solutions:

(a) A solution for a line dislocation perpendicular to $x_1 - x_2$ plane in an infinite plane without crack;
(b) A disturbed solution due to the presence of the crack. For the solution, the opposite tractions deduced by the line dislocations are applied to the crack surfaces.

To model the crack kinking behavior, the kinked segment of length a is replaced by a continuous distribution of dislocations. The net tractions on the kinked surfaces resulting from distribution of the dislocations and the remote loading should be zero. This results in a system of singular integral equations.

3. Crack kinking analysis

In the Stroh formalism, the solution (a) for a line dislocation with Burgers vector $\hat{\boldsymbol{b}}$ located at (x_{10}, x_{20}) in an infinite plane without crack is given by

$$\boldsymbol{\Phi}(z) = \frac{1}{2\pi} \boldsymbol{B} \langle \ln(z - z_0) \rangle \boldsymbol{B}^{-1} \boldsymbol{q}_0 \tag{3.1}$$

$$\boldsymbol{u} = \mathrm{Re}\left[\boldsymbol{A}\boldsymbol{B}^{-1}\boldsymbol{\Phi}(z)\right] = \frac{1}{2\pi} \mathrm{Re}\left[\boldsymbol{A} \langle \ln(z - z_0) \rangle \boldsymbol{B}^{-1} \boldsymbol{q}_0\right] \tag{3.2}$$

$$\boldsymbol{t}_1 = [\sigma_{11}, \sigma_{12}, \sigma_{13}]^{\mathrm{T}} = -\mathrm{Re}\big[\boldsymbol{\Phi}_{,2}\big], \qquad \boldsymbol{t}_2 = [\sigma_{12}, \sigma_{22}, \sigma_{23}]^{\mathrm{T}} = \mathrm{Re}\big[\boldsymbol{\Phi}_{,1}\big] \tag{3.3}$$

where

$$\boldsymbol{q}_0 = \boldsymbol{L}\hat{\boldsymbol{b}}$$

$$\langle \ln(z - z_0)\rangle = \mathrm{diag}\big[\ln(z_1 - z_{10}), \ln(z_2 - z_{20}), \ln(z_3 - z_{30})\big]$$

$$z_\alpha = x_1 + p_\alpha x_2, \quad z_{\alpha 0} = x_{10} + p_\alpha x_{20} \tag{3.4}$$

$\boldsymbol{\Phi}$ is the complex stress function or complex potential, $p_\alpha, \boldsymbol{A}, \boldsymbol{B}$ are the Stroh eigenvalues and matrices (Ting, 1996). They depend on elastic constants only. $\boldsymbol{L} = -2i\boldsymbol{B}\boldsymbol{B}^{\mathrm{T}}$ is a real, symmetric matrix. From Eq. (3.1), the traction on the plane $x_2 = 0$ with unit normal $[0, 1, 0]^{\mathrm{T}}$ is

$$\boldsymbol{t}_2(x_1) = \mathrm{Re}\big[\boldsymbol{\Phi}'(z)\big]\Big|_{x_2=0}, \tag{3.5a}$$

$$\boldsymbol{\Phi}'(z) = \frac{1}{2\pi}\boldsymbol{B}\Big\langle\frac{1}{z - z_0}\Big\rangle\boldsymbol{B}^{-1}\boldsymbol{q}_0 \tag{3.5b}$$

Here, the prime denotes the derivative with respect to the associated arguments.

The solution (b) is investigated next. Consider a semi-infinite crack located on plane $x_2 = 0$ and $x_1 < 0$. The traction $-\boldsymbol{t}_2$ from Eq. (3.5a) is applied on the lower crack surface and $\boldsymbol{t}_2$ on the upper crack surface. Solving this problem leads to a Hilbert equation. The derivative of the complex potential for the semi-infinite crack with the prescribed tractions on the faces can be written, in Stroh formalism,

$$\boldsymbol{\Phi}'(z) = -\frac{1}{4\pi}\left[\boldsymbol{B}\Big\langle\frac{1 - \sqrt{z_0/z}}{z - z_0}\Big\rangle\boldsymbol{B}^{-1} + \sum_{\beta=1}^{3}\boldsymbol{B}\Big\langle\frac{1 - \sqrt{\bar{z}_{\beta 0}/z}}{z - \bar{z}_{\beta 0}}\Big\rangle\boldsymbol{Y}_\beta\right]\boldsymbol{q}_0 \tag{3.6}$$

$$\boldsymbol{Y}_\beta = \boldsymbol{B}^{-1}\bar{\boldsymbol{B}}\mathbf{I}_\beta\bar{\boldsymbol{B}}^{-1} \tag{3.7}$$

where

$$\mathbf{I}_1 = \mathrm{diag}[1, 0, 0], \quad \mathbf{I}_2 = \mathrm{diag}[0, 1, 0], \quad \mathbf{I}_3 = \mathrm{diag}[0, 0, 1]$$

$$\Big\langle\frac{1 - \sqrt{z_0/z}}{z - z_0}\Big\rangle = \mathrm{diag}\left[\frac{1 - \sqrt{z_{10}/z_1}}{z_1 - z_{10}}, \frac{1 - \sqrt{z_{20}/z_2}}{z_2 - z_{20}}, \frac{1 - \sqrt{z_{30}/z_3}}{z_3 - z_{30}}\right]$$

$$\Big\langle\frac{1 - \sqrt{\bar{z}_{\beta 0}/z}}{z - \bar{z}_{\beta 0}}\Big\rangle = \mathrm{diag}\left[\frac{1 - \sqrt{\bar{z}_{\beta 0}/z_1}}{z_1 - \bar{z}_{\beta 0}}, \frac{1 - \sqrt{\bar{z}_{\beta 0}/z_2}}{z_2 - \bar{z}_{\beta 0}}, \frac{1 - \sqrt{\bar{z}_{\beta 0}/z_3}}{z_3 - \bar{z}_{\beta 0}}\right]$$

Superimposing the two solutions, (3.5b) and (3.6), the derivative of the complex stress function and displacement for the line dislocation interacting with the traction-free crack are given by

$$\boldsymbol{\Phi}'(z) = \boldsymbol{\Phi}'_0 + \boldsymbol{\Phi}'_T = \frac{1}{2\pi}\left[\boldsymbol{B}\langle\frac{1}{z-z_0}\rangle\boldsymbol{B}^{-1} - \frac{1}{2}\boldsymbol{B}\langle\frac{1-\sqrt{z_0/z}}{z-z_0}\rangle\boldsymbol{B}^{-1} - \frac{1}{2}\sum_{\beta=1}^{3}\boldsymbol{B}\langle\frac{1-\sqrt{\bar{z}_{\beta 0}/z}}{z-\bar{z}_{\beta 0}}\rangle\boldsymbol{Y}_\beta\right]\boldsymbol{q}_0 \tag{3.8a}$$

$$\boldsymbol{u} = \mathrm{Re}\left[\boldsymbol{A}\boldsymbol{B}^{-1}\boldsymbol{\Phi}(z)\right] \tag{3.8b}$$

where the subscripts 0 and T denote the solutions Eqs. (3.5) and (3.6) for line dislocation and crack with prescribed tractions, respectively. The expression for this fundamental solution $\boldsymbol{\Phi}(z)$ is readily obtained by integrating Eq. (3.8a) with respect to z.

The next step in the analysis involves the formulation of the kinked crack shown in Fig. 1. This is accomplished by simulating the kinked segment by a continuous distribution of dislocations. It is convenient to use the cylindrical coordinate system (r, θ, x_3) where

$$x_1 = r\cos\theta, \qquad x_2 = r\sin\theta$$

$$x_{10} = r_0\cos\omega, \qquad x_{20} = r_0\sin\omega, \quad 0 \le r_0 \le a$$

and r_0 is the distance from the origin to (x_{10}, x_{20}).

For a single line dislocation located at (x_{10}, x_{20}) on the segment, the complex potential is given by Eq. (3.8a) in which

$$z_\alpha = r(\cos\theta + p_\alpha\sin\theta)$$

$$z_{\alpha 0} = r_0(\cos\omega + p_\alpha\sin\omega), \quad 0 \le r_0 \le a \tag{3.9}$$

Replacing $\boldsymbol{q}_0$ by $\boldsymbol{q}_{\mathrm{D}}(r_0)\mathrm{d}r_0$ in Eq. (3.8a) and integrating with respect to r_0 from 0 to a, we get the potential for the distributions of dislocation interacting with the crack given by the integral expansion

$$\boldsymbol{\Phi}'_D(z) = \frac{1}{2\pi}\int_0^a\left[\boldsymbol{B}\langle\frac{1}{z-z_0}\rangle\boldsymbol{B}^{-1} - \frac{1}{2}\boldsymbol{B}\langle\frac{1-\sqrt{z_0/z}}{z-z_0}\rangle\boldsymbol{B}^{-1} - \frac{1}{2}\sum_{\beta=1}^{3}\boldsymbol{B}\langle\frac{1-\sqrt{\bar{z}_{\beta 0}/z}}{z-\bar{z}_{\beta 0}}\rangle\boldsymbol{Y}_\beta\right]\boldsymbol{q}_D(r_0)\,\mathrm{d}r_0 \tag{3.10}$$

where $\boldsymbol{q}_{\mathrm{D}}(r_0)$ is the dislocation density.

For the crack kinking problem, the dislocation density $\boldsymbol{q}_{\mathrm{D}}(r_0)$ is unknown. However, the unknown function $\boldsymbol{q}_{\mathrm{D}}(r_0)$ must lead to the traction-free condition along the kinked crack surfaces

$$\boldsymbol{t}_\theta|_{\theta=\omega} = \left(\boldsymbol{t}_\theta^{\mathrm{D}} + \boldsymbol{t}_\theta^{\mathrm{L}}\right)|_{\theta=\omega} = 0, \quad 0 < r < a \tag{3.11}$$

where $\boldsymbol{t}_\theta$ is the traction on $\theta =$ constant, the superscripts (or subscripts) D and L denote the quantities induced by the distribution of dislocations and the loading applied to the main crack, respectively.

The traction vector $\boldsymbol{t}_\theta$ on a radial plane $\theta =$ constant is given by

$$\boldsymbol{t}_\theta = \mathrm{Re}\left[\frac{\partial\boldsymbol{\Phi}}{\partial r}\right] \tag{3.12}$$

Denote the complex potential for the main crack tip by $\boldsymbol{\Phi}_{\mathrm{L}}$ under loading $\boldsymbol{k}$, $\boldsymbol{T}$, and $\boldsymbol{g}$. Then

$$\boldsymbol{\Phi}_{\mathrm{L}} = \sqrt{\frac{2}{\pi}}\boldsymbol{B}\langle\sqrt{z}\rangle\boldsymbol{B}^{-1}\boldsymbol{k} + \boldsymbol{B}\langle z\rangle\boldsymbol{B}^{-1}\boldsymbol{g}_0 + \frac{2}{3}\sqrt{\frac{2}{\pi}}\boldsymbol{B}\langle z^{3/2}\rangle B^{-1}\boldsymbol{g} + O(z^2) \tag{3.13}$$

where $\boldsymbol{T} = -\mathrm{Re}[\boldsymbol{B}\langle p\rangle\boldsymbol{B}^{-1}\boldsymbol{g}_0]$ and $\mathrm{Re}[\boldsymbol{g}_0] = 0$.

From Eqs. (3.10), (3.12) and (3.13)

$$\boldsymbol{t}_{\omega}^{D} = \boldsymbol{t}_{\theta}^{\mathrm{D}}|_{\theta=\omega} = \frac{1}{2\pi}\int_0^a \left[\frac{\mathbf{I}}{r-r_0} - \frac{1}{2}\frac{\mathbf{I}}{r+\sqrt{rr_0}} - \frac{1}{2}\sum_{\beta=1}^{3}\mathrm{Re}\left[\boldsymbol{B}\langle\frac{1}{r+\sqrt{rr_0\bar{\varsigma}_\beta/\varsigma}}\rangle\boldsymbol{Y}_\beta\right]\right]\boldsymbol{q}_{\mathrm{D}}(r_0)\,\mathrm{d}r_0 \tag{3.14}$$

$$\boldsymbol{t}_{\omega}^{\mathrm{L}} = \frac{1}{\sqrt{2\pi r}}\mathrm{Re}\big[\boldsymbol{B}\langle\sqrt{\varsigma}\rangle\boldsymbol{B}^{-1}\big]\boldsymbol{k} - \sin\omega\boldsymbol{T} + \sqrt{\frac{2r}{\pi}}\mathrm{Re}\big[\boldsymbol{B}\langle\varsigma^{3/2}\rangle\boldsymbol{B}^{-1}\big]\boldsymbol{g} + O(r^2) \tag{3.15}$$

where $\varsigma_\alpha = \cos\omega + p_\alpha\sin\omega$, $r = \sqrt{x_1^2 + x_2^2}$, $r_0 = \sqrt{x_{10}^2 + x_{20}^2}$.

Substituting Eqs. (3.14) and (3.15) into Eq. (3.11) leads to

$$\frac{1}{2\pi}\int_0^a \left[\frac{\mathbf{I}}{r_0-r} + \frac{1}{2}\frac{\mathbf{I}}{r+\sqrt{rr_0}} + \frac{1}{2}\sum_{\beta=1}^{3}\mathrm{Re}\left[\boldsymbol{B}\langle\frac{1}{r+\sqrt{rr_0\bar{\varsigma}_\beta/\varsigma}}\rangle\boldsymbol{Y}_\beta\right]\right]\boldsymbol{q}_{\mathrm{D}}\,\mathrm{d}r_0$$

$$= \frac{1}{\sqrt{2\pi r}}\mathrm{Re}\big[\boldsymbol{B}\langle\sqrt{\varsigma}\rangle\boldsymbol{B}^{-1}\big]\boldsymbol{k} - \sin\omega\boldsymbol{T} + \sqrt{\frac{2r}{\pi}}\mathrm{Re}\big[\boldsymbol{B}\langle\varsigma^{3/2}\rangle\boldsymbol{B}^{-1}\big]\boldsymbol{g} + O(r^2) \tag{3.16}$$

This is a system of singular integral equations for the dislocation density $\boldsymbol{q}_{\mathrm{D}}(r_0)$ and it governs the crack kinking problem. It is convenient to introduce the nondimensional variables x ant t such that

$$r = \frac{a}{2}(1+x), \qquad r_0 = \frac{a}{2}(1+t) \tag{3.17}$$

Assume $\boldsymbol{q}_{\mathrm{D}}$ has the form

$$\boldsymbol{q}_{\mathrm{D}} = \frac{2\pi(1+t)^{-s}(1-t)^{-1/2}\boldsymbol{q}(t)}{\sqrt{a}} \tag{3.18}$$

where $\boldsymbol{q}(t)$ is a unknown function bounded on $-1 \le t \le 1$ (Note that $\boldsymbol{q}(t)$ has dimension of the stress intensity factor), $-1/2$ and $-s(\omega; s'_{ij})$ are the stress singularity at the kink tip and the kink corner, respectively. Then the integral equation (3.16) is written as

$$\int_{-1}^{1}\frac{\mathbf{I}}{t-x} + \frac{1}{2}\frac{\mathbf{I}}{1+x+\sqrt{(1+x)(1+t)}}$$

$$+ \frac{1}{2}\sum_{\beta=1}^{3}\mathrm{Re}\left[\boldsymbol{B}\langle\frac{1}{1+x+\sqrt{(1+x)(1+t)\bar{\varsigma}_\beta/\varsigma}}\rangle\boldsymbol{Y}_\beta\right]\frac{\boldsymbol{q}(t)\,\mathrm{d}t}{(1+t)^s(1-t)^{1/2}}$$

$$= \frac{1}{\sqrt{\pi(1+x)}}\mathrm{Re}\big[\boldsymbol{B}\langle\sqrt{\varsigma}\rangle\boldsymbol{B}^{-1}\big]\boldsymbol{k} - \sqrt{a}\boldsymbol{T}\sin\omega + a\sqrt{\frac{1+x}{\pi}}\mathrm{Re}\big[\boldsymbol{B}\langle\varsigma^{3/2}\rangle\boldsymbol{B}^{-1}\big]\boldsymbol{g} \tag{3.19}$$

Eq. (3.19) can be rewritten in a standard form

$$\int_{-1}^{1} \frac{w(t)\boldsymbol{q}(t)\,\mathrm{d}t}{t-x} + \int_{-1}^{1} \boldsymbol{K}(x,t)w(t)\boldsymbol{q}(t)\,\mathrm{d}t = f(x), \quad -1 < x < 1 \tag{3.20}$$

where the first integral on the left-hand side is the dominant part,

$$w(t) = (1+t)^{-s}(1-t)^{-1/2} \tag{3.21}$$

The matrix $\boldsymbol{K}(x, t)$ is the known function which contains the second and the third terms in the integrand in Eq. (3.19), $\boldsymbol{f}(x)$ consists of the k-term, T-term, g-term, etc.. The equation can be solved using different numerical techniques as given by Erdogan et al. (1973), He and Hutchinson (1989) and Erdogan and Gupta (1972). In these approaches, the unknown function $\boldsymbol{q}(t)$ is expanded in terms of Chebychev polynomials or Jacobi polynomials with unknown coefficients. This results in a system of linear algebraic equations for $\boldsymbol{q}(t)$. In this paper, a series of Chebychev polynomial is used, $s = 1/2$ and the condition $\boldsymbol{q}(-1) = 0$ are imposed at the kinked corner. In calculation the series is truncated at $(N + 1)$th term $(N = 120)$. Comparing the results with the existing results given by Melin (1994) and Khrapkov (1998) for isotropic materials and Suo et al. (1991) for orthotropic materials, a very good agreement has been achieved.

Since the integral equation is linear in $\boldsymbol{q}(t)$, the solution for $\boldsymbol{q}(t)$ can be obtained by superposition of the solutions due to k-term, T-term, and the other higher-order terms. From Eq. (3.19) or Eq. (3.20), the solution $\boldsymbol{q}(t)$ can be expressed by

$$\boldsymbol{q}(t) = k_2\boldsymbol{q}_2^{(1)}(t) + k_1\boldsymbol{q}_1^{(1)}(t) + k_3\boldsymbol{q}_3^{(1)}(t) + \sqrt{a}T_1\boldsymbol{q}_1^{(2)}(t) + \sqrt{a}T_3\boldsymbol{q}_3^{(2)}(t) + a\sum_{i=1}^{3}\boldsymbol{q}_i^{(3)}(t)g_i \tag{3.22}$$

where the eight terms represent the contribution to $\boldsymbol{q}(t)$ due to k_2, k_1, k_3, T_1, T_3, g_i respectively. The superscripts (i), $i = 1, 2, 3$ denote the terms created by k-term, T-term, and g-term, respectively. $\boldsymbol{q}_2^{(1)}$, $\boldsymbol{q}_1^{(1)}$, $\boldsymbol{q}_3^{(1)}$ can be obtained from solving integral equations

$$\int_{-1}^{1} \frac{w(t)\boldsymbol{q}(t)}{t-x}\,\mathrm{d}t + \int_{-1}^{1} \boldsymbol{K}(x,t)w(t)\boldsymbol{q}(t)\,\mathrm{d}t = \frac{1}{\sqrt{\pi(1+x)}}\mathrm{Re}\left[\boldsymbol{B}\langle\sqrt{\varsigma}\rangle\boldsymbol{B}^{-1}\right]\boldsymbol{k} \tag{3.23}$$

by setting $\boldsymbol{k} = [1, 0, 0]^{\mathrm{T}}$, $[0, 1, 0]^{\mathrm{T}}$ and $[0, 0, 1]^{\mathrm{T}}$ in Eq. (3.23), respectively, while $\boldsymbol{q}_1^{(2)}$ and $\boldsymbol{q}_3^{(2)}$ can be calculated from solving the integral equation

$$\int_{-1}^{1} \frac{w(t)\boldsymbol{q}(t)}{t-x}\,\mathrm{d}t + \int_{-1}^{1} \boldsymbol{K}(x,t)w(t)\boldsymbol{q}(t)\,\mathrm{d}t = -\sqrt{a}\boldsymbol{T}\sin\omega \tag{3.24}$$

by choosing $\boldsymbol{T} = [1, 0, 0]^{\mathrm{T}}$ and $[0, 0, 1]^{\mathrm{T}}$ in Eq. (3.24), respectively. $\boldsymbol{q}_2^{(3)}$, $\boldsymbol{q}_1^{(3)}$, $\boldsymbol{q}_3^{(3)}$ are determined from

$$\int_{-1}^{1} \frac{w(t)\boldsymbol{q}(t)}{t-x}\,\mathrm{d}t + \int_{-1}^{1} \boldsymbol{K}(x,t)w(t)\boldsymbol{q}(t)\,\mathrm{d}t = a\sqrt{\frac{1+x}{\pi}}\mathrm{Re}\left[\boldsymbol{B}\langle\varsigma^{3/2}\rangle\boldsymbol{B}^{-1}\right]\boldsymbol{g} \tag{3.25}$$

with selecting $\boldsymbol{g} = [1, 0, 0]^{\mathrm{T}}$, $[0, 1, 0]^{\mathrm{T}}$ and $[0,0,1]^{\mathrm{T}}$, respectively.

The contributions to $\boldsymbol{q}(t)$ due to other higher-order terms can be determined in a similar procedure. The solution of $\boldsymbol{q}(t)$ can be used to calculate the stress intensity factors, T-stresses, and energy release rate as given in the following sections.

Note that the solution for the integral equations is valid if the crack surfaces are traction-free for both the main crack and kinked crack. This requires that the crack surfaces are open. For the main crack, the displacements due to the singular term are expressed by

$$\boldsymbol{u} = \sqrt{\frac{2}{\pi}}\mathrm{Re}\left[\boldsymbol{A}\langle\sqrt{z}\rangle\boldsymbol{B}^{-1}\right]\boldsymbol{k} \tag{3.26}$$

It follows that the crack opening displacement

$$\Delta u_2 = u_2(r,\pi) - u_2(r,-\pi) = 2\sqrt{\frac{2r}{\pi}}[\boldsymbol{L}^{-1}\boldsymbol{k}]_2 \tag{3.27}$$

where $[\ ]_2$ denotes the second element of the vector inside the bracket. The open crack tip implies that $[\boldsymbol{L}^{-1}\boldsymbol{k}]_2 \geq 0$. Similarly, for the kinked crack, the traction-free condition on the crack tip requires

$$\left[\boldsymbol{L}_{\omega}^{-1}\boldsymbol{k}'\right]_2 \geq 0 \tag{3.28}$$

where $\boldsymbol{L}_{\omega}^{-1}$ is the matrix referred to the coordinate (x_1', x_2', x_3') system located at the kinked crack tip shown in Fig. 1.

4. Stress intensity factors at the kinked tip

The stress intensity factors at the kink tip are defined by

$$\boldsymbol{k}' = \lim_{r\to a}\sqrt{2\pi(r-a)}\left\{\begin{array}{c}\sigma_{r\theta}\\ \sigma_{\theta\theta}\\ \sigma_{3\theta}\end{array}\right\}_{\theta=\omega}, \quad r > a \tag{4.1}$$

Since

$$\left\{\begin{array}{c}\sigma_{r\theta}\\ \sigma_{\theta\theta}\\ \sigma_{3\theta}\end{array}\right\}_{\theta=\omega} = \boldsymbol{\Omega}\boldsymbol{t}_{\theta}|_{\theta=\omega}, \qquad \boldsymbol{\Omega} = \begin{bmatrix}\cos\omega & \sin\omega & 0\\ -\sin\omega & \cos\omega & 0\\ 0 & 0 & 1\end{bmatrix} \tag{4.2}$$

$\boldsymbol{k}'$can be expressed by

$$\boldsymbol{k}' = \lim_{r\to a}\sqrt{2\pi(r-a)}\boldsymbol{\Omega}\boldsymbol{t}_{\theta}|_{\theta=\omega} = \lim_{x\to 1}\sqrt{\pi a(x-1)}\boldsymbol{\Omega}\boldsymbol{t}_{\theta}|_{\theta=\omega}, \quad x > 1 \tag{4.3}$$

It can be shown that as $x\to 1$, the contribution to $\boldsymbol{k}'$ only comes from the dominant term in the expression of $\boldsymbol{t}_{\theta}|_{\theta=\omega}$, the limiting value can be evaluated using a technique given by Muskhelishvili (1953) and

$$\lim_{x\to 1}\boldsymbol{t}_{\theta}|_{\theta=\omega} = \lim_{x\to 1}\frac{1}{\sqrt{a}}\int_{-1}^{1}\frac{\boldsymbol{q}(t)\,\mathrm{d}t}{(x-t)(1+t)^{s}(1-t)^{1/2}} = \frac{\pi\boldsymbol{q}(1)}{2^{s}\sqrt{a(x-1)}} \tag{4.4}$$

Hence

$$\boldsymbol{k}' = \frac{\pi\sqrt{\pi}}{2^{s}}\boldsymbol{\Omega}\boldsymbol{q}(1) \tag{4.5}$$

Once the numerical solutions $\boldsymbol{q}_2^{(1)}$, $\boldsymbol{q}_1^{(1)}$, $\boldsymbol{q}_3^{(1)}$, $\boldsymbol{q}_1^{(2)}$, $\boldsymbol{q}_3^{(2)}$, $\boldsymbol{q}_2^{(3)}$, $\boldsymbol{q}_1^{(3)}$, and $\boldsymbol{q}_3^{(3)}$ are known from (3.23)–(3.25), according to Eqs. (3.22) and (4.5), $\boldsymbol{k}'$ can be expressed in terms of $\boldsymbol{k}$, $\boldsymbol{T}$, and $\boldsymbol{g}$ in the form

$$\begin{bmatrix} k_2' \\ k_1' \\ k_3' \end{bmatrix} = \begin{bmatrix} c_{22} & c_{21} & c_{23} \\ c_{12} & c_{11} & c_{13} \\ c_{32} & c_{31} & c_{33} \end{bmatrix} \begin{bmatrix} k_2 \\ k_1 \\ k_3 \end{bmatrix} + \sqrt{a} T_1 \begin{bmatrix} b_{21} \\ b_{11} \\ b_{31} \end{bmatrix} + \sqrt{a} T_3 \begin{bmatrix} b_{23} \\ b_{13} \\ b_{33} \end{bmatrix} + a \begin{bmatrix} h_{22} & h_{21} & h_{23} \\ h_{12} & h_{11} & h_{13} \\ h_{32} & h_{31} & h_{33} \end{bmatrix} \begin{bmatrix} g_2 \\ g_1 \\ g_3 \end{bmatrix} \tag{4.6}$$

or

$$\boldsymbol{k}' = \boldsymbol{c}\boldsymbol{k} + \sqrt{a}\boldsymbol{b}\boldsymbol{T} + a\boldsymbol{h}\boldsymbol{g} \tag{4.7}$$

where

$$\boldsymbol{c} = \frac{\pi\sqrt{\pi}}{2^s}\boldsymbol{\Omega}\left[\boldsymbol{q}_2^{(1)}(1), \boldsymbol{q}_1^{(1)}(1), \boldsymbol{q}_3^{(1)}(1)\right], \tag{4.8}$$

$$\boldsymbol{b} = [\boldsymbol{b}_1, 0, \boldsymbol{b}_3], \quad \boldsymbol{b}_1 = \begin{bmatrix} b_{21} \\ b_{11} \\ b_{31} \end{bmatrix} = \frac{\pi\sqrt{\pi}}{2^s}\boldsymbol{\Omega}\boldsymbol{q}_1^{(2)}(1), \quad \boldsymbol{b}_3 = \begin{bmatrix} b_{23} \\ b_{13} \\ b_{33} \end{bmatrix} = \frac{\pi\sqrt{\pi}}{2^s}\boldsymbol{\Omega}\boldsymbol{q}_3^{(2)}(1), \tag{4.9}$$

$$\boldsymbol{h} = \frac{\pi\sqrt{\pi}}{2^s}\boldsymbol{\Omega}\left[\boldsymbol{q}_2^{(3)}(1), \boldsymbol{q}_1^{(3)}(1), \boldsymbol{q}_3^{(3)}(1)\right] \tag{4.10}$$

Following a similar manner, $\boldsymbol{k}'$ induced by other higher-order terms can be obtained.

5. *T*-stresses at the kinked tip

Referring to the coordinate system (x_1', x_2', x_3') attached to the kinked tip shown in Fig. 1, the asymptotic stress field near the tip is

$$\sigma_{\alpha\beta}' = \sigma'^{(0)}_{\alpha\beta}(r', \theta') + T_1'\delta_{\alpha1}\delta_{\beta1} + T_3'\delta_{\alpha3}\delta_{\beta1} + O(\sqrt{r'}), \quad \sigma_{\alpha\beta} \neq \sigma_{33} \tag{5.1}$$

where the superscript prime denotes the quantities referred to the (x_1', x_2', x_3') system, $\sigma'^{(0)}_{\alpha\beta}$ is the singular term with $\sigma'^{(0)}_{\alpha\beta} \propto 1/\sqrt{r'}$, $r' = \sqrt{x'^2_1 + x'^2_2}$, $r'\cos\theta' = x_1'$, $r'\sin\theta' = x_2'$.

By the definition of *T*-stresses

$$T_1' = \lim_{r' \to 0}\left(\sigma_{11}' - \sigma'^{(0)}_{11}\right)|_{\theta'=0}, \qquad T_3' = \lim_{r' \to 0}\left(\sigma_{31}' - \sigma'^{(0)}_{31}\right)|_{\theta'=0} \tag{5.2}$$

Note that the constant term of σ_{12}' is zero. Let σ_{rr}, $\sigma_{r\theta}$, σ_{r3} be the cylindrical components of the stress on r = constant. Then

$$\begin{bmatrix} \sigma_{11}' \\ \sigma_{21}' \\ \sigma_{31}' \end{bmatrix}_{\theta=0} = \begin{bmatrix} \sigma_{rr} \\ \sigma_{r\theta} \\ \sigma_{r3} \end{bmatrix}_{\theta=\omega}, \quad r > a \tag{5.3}$$

Thus

$$T_1' = \lim_{r \to a}\left(\sigma_{rr} - \sigma_{rr}^{(0)}\right)|_{\theta=\omega}, \qquad T_3' = \lim_{r \to a}\left(\sigma_{r3} - \sigma_{r3}^{(0)}\right)|_{\theta=\omega} \tag{5.4}$$

where $\sigma_{rr}^{(0)}$ and $\sigma_{r3}^{(0)}$ are the leading terms of σ_{rr} and σ_{r3}, respectively. Because

$$\begin{bmatrix}\sigma_{rr}\\ \sigma_{r\theta}\\ \sigma_{r3}\end{bmatrix} = \boldsymbol{\Omega}(\theta)\boldsymbol{t}_r \qquad \boldsymbol{\Omega}(\theta) = \begin{bmatrix}\cos\theta & \sin\theta & 0\\ -\sin\theta & \cos\theta & 0\\ 0 & 0 & 1\end{bmatrix} \tag{5.5}$$

and

$$\boldsymbol{t}_r = -\frac{1}{r}Re\left[\frac{\partial\boldsymbol{\Phi}}{\partial\theta}\right], \quad \boldsymbol{\Phi} = \boldsymbol{\Phi}_{\mathrm{D}} + \boldsymbol{\Phi}_{\mathrm{L}} \tag{5.6}$$

Finally, we have the expression, via Eqs. (5.3), (5.5), (5.6) and (3.17)

$$[\sigma_{rr}, \sigma_{r\theta}, \sigma_{r3}]^{\mathrm{T}}|_{\theta=\omega} = \frac{\boldsymbol{\Omega}(\omega)}{\sqrt{a}}\mathrm{Re}\{\boldsymbol{B}\langle p(\omega)\rangle\boldsymbol{B}^{-1}\int_{-1}^{1}\frac{w(t)\boldsymbol{q}(t)}{t-x}\,\mathrm{d}t$$

$$+\frac{1}{2}\boldsymbol{B}\langle p(\omega)\rangle\boldsymbol{B}^{-1}\int_{-1}^{1}\frac{w(t)\boldsymbol{q}(t)}{1+x+\sqrt{(1+x)(1+t)}}\,\mathrm{d}t$$

$$+\frac{1}{2}\sum_{\beta=1}^{3}\int_{-1}^{1}\boldsymbol{B}\langle\frac{p(\omega)}{1+x+\sqrt{(1+x)(1+t)}\varsigma_\beta/\varsigma}\rangle\boldsymbol{Y}_\beta w(t)\boldsymbol{q}(t)\,\mathrm{d}t, \quad x>1$$

$$-\frac{1}{\sqrt{\pi(1+x)}}\boldsymbol{B}\langle p(\omega)\sqrt{\varsigma}\rangle\boldsymbol{B}^{-1}\boldsymbol{k} + \sqrt{a}\boldsymbol{T}\cos\omega\} \tag{5.7}$$

$$\left[\sigma_{rr}^{(0)}, \sigma_{r\theta}^{(0)}, \sigma_{r3}^{(0)}\right]^{\mathrm{T}}|_{\theta=\omega} = \frac{\boldsymbol{\Omega}(\omega)}{\sqrt{a}}\mathrm{Re}\left[\boldsymbol{B}\langle p(\omega)\rangle\boldsymbol{B}^{-1}\frac{\pi\boldsymbol{q}(1)}{2^s\sqrt{x-1}}\right], \quad x>1 \tag{5.8}$$

where

$$\langle p(\omega)\rangle = \mathrm{diag}\left[p_1(\omega), p_2(\omega), p_3(\omega)\right]$$

$$p_\alpha(\omega) = \frac{-\sin\omega + p_\alpha\cos\omega}{\cos\omega + p_\alpha\sin\omega}, \quad \varsigma_\alpha = \cos\omega + p_\alpha\sin\omega \tag{5.9}$$

From Eqs. (5.4), (5.7) and (5.8),

$$\boldsymbol{T}' = \left[T_1', 0, T_3'\right]^{\mathrm{T}} = \frac{\boldsymbol{\Omega}(\omega)}{\sqrt{a}}\left\{\boldsymbol{m} - \frac{1}{\sqrt{2\pi}}\mathrm{Re}\left[\boldsymbol{B}\langle p(\omega)\sqrt{\varsigma}\rangle\boldsymbol{B}^{-1}\boldsymbol{k}\right] + \sqrt{a}\boldsymbol{T}\cos\omega\right\} \tag{5.10}$$

where

$$\boldsymbol{m} = \mathrm{Re}\{\boldsymbol{B}\langle p(\omega)\rangle\boldsymbol{B}^{-1}\lim_{x\to1}\left[\int_{-1}^{1}\frac{w(t)\boldsymbol{q}(t)}{t-x}\,\mathrm{d}t - \frac{\pi\boldsymbol{q}(1)}{2^s\sqrt{x-1}}\right]$$

$$+\frac{1}{2}\boldsymbol{B}\langle p(\omega)\rangle\boldsymbol{B}^{-1}\int_{-1}^{1}\frac{w(t)\boldsymbol{q}(t)}{2+\sqrt{2(1+t)}}\,\mathrm{d}t$$

$$+\frac{1}{2}\sum_{\beta=1}^{3}\int_{-1}^{1}\boldsymbol{B}\langle\frac{p(\omega)}{2+\sqrt{2(1+t)\varsigma_\beta/\varsigma}}\rangle\boldsymbol{Y}_\beta w(t)\boldsymbol{q}(t)\,\mathrm{d}t\} \tag{5.11}$$

Eq. (5.10) provides the evaluation of T-stress from the radial stress at the front of the kinked tip ($\theta'=0$). With Eqs. (5.10) and (3.22), $\boldsymbol{T}'$ is related to $\boldsymbol{k}$ and $\boldsymbol{T}$ by the relation

$$\begin{bmatrix} T_1' \\ 0 \\ T_3' \end{bmatrix} = \frac{1}{\sqrt{a}}\begin{bmatrix} d_{12} & d_{11} & d_{13} \\ 0 & 0 & 0 \\ d_{32} & d_{31} & d_{33} \end{bmatrix}\begin{bmatrix} k_2 \\ k_1 \\ k_3 \end{bmatrix} + \begin{bmatrix} e_{11} & 0 & e_{13} \\ 0 & 0 & 0 \\ e_{31} & 0 & e_{33} \end{bmatrix}\begin{bmatrix} T_1 \\ 0 \\ T_3 \end{bmatrix} \tag{5.12}$$

or

$$\boldsymbol{T}' = \boldsymbol{d}\boldsymbol{k}/\sqrt{a} + \boldsymbol{e}\boldsymbol{T}$$

where

$$\boldsymbol{d} = \boldsymbol{\Omega}\left\{\left[\boldsymbol{m}_2^{(1)}, \boldsymbol{m}_1^{(1)}, \boldsymbol{m}_3^{(1)}\right] - \mathrm{Re}\left[\boldsymbol{B}\langle p(\omega)\sqrt{\varsigma}\rangle\boldsymbol{B}^{-1}\right]\right\}$$

$$\boldsymbol{e} = \boldsymbol{\Omega}\left\{\left[\boldsymbol{m}_1^{(2)}, 0, \boldsymbol{m}_3^{(2)}\right] + [\boldsymbol{e}_1, 0, \boldsymbol{e}_3]\cos\omega\right\}$$

$$\boldsymbol{e}_1 = [1, 0, 0]^{\mathrm{T}}, \qquad e_3 = [0, 0, 1]^{\mathrm{T}}$$

$\boldsymbol{m}_2^{(1)}$, $\boldsymbol{m}_1^{(1)}$, $\boldsymbol{m}_3^{(1)}$, $\boldsymbol{m}_1^{(2)}$, $\boldsymbol{m}_3^{(2)}$ are evaluated from Eq. (5.11) by choosing $\boldsymbol{q}(t)=\boldsymbol{q}_2^{(1)}$, $\boldsymbol{q}_1^{(1)}$, $\boldsymbol{q}_3^{(1)}$, $\boldsymbol{q}_1^{(2)}$, $\boldsymbol{q}_3^{(2)}$, respectively.

For simplicity, Eq. (5.12) can be reduced to the form in Eq. (2.4). Note that the T-stress can also be calculated from the radial stress on the flanks of the kinked crack.

6. Energy release rate at the kinked tip

The energy release rate for the main crack extension in x_1-direction prior to kinking is

$$G_0 = G(\omega)|_{\substack{\omega=0\\ a\to 0}} = \frac{1}{2}\boldsymbol{k}^{\mathrm{T}}\boldsymbol{L}^{-1}\boldsymbol{k} = \frac{|\boldsymbol{k}|^2}{2}\boldsymbol{n}^{\mathrm{T}}\boldsymbol{L}^{-1}\boldsymbol{n} \tag{6.1}$$

where $\boldsymbol{k}=|\boldsymbol{k}|\boldsymbol{n}$, $\boldsymbol{n}=[\sin\phi\sin\psi, \sin\phi\cos\psi, \cos\psi]^{\mathrm{T}}$, $|\boldsymbol{k}|=\sqrt{k_2^2+k_1^2+k_3^2}$,

$$\tan\psi = \frac{k_2}{k_1}, \qquad \cos\phi = \frac{k_3}{|\boldsymbol{k}|} \tag{6.2}$$

$\boldsymbol{n}$ is the direction cosine of $\boldsymbol{k}$ in the (k_2, k_1, k_3) space. ψ is a measure of relative magnitude of mode-II to mode-I of the loading on the main crack; ϕ is the ratio of magnitude of mode-III to the norm of the stress intensity factor at the main crack, $\boldsymbol{L}^{-1}(=\mathrm{Re}[i\boldsymbol{A}\boldsymbol{B}^{-1}])$ is a tensor of rank two referred to (x_1, x_2, x_3) system,

The energy release rate of the crack kinking at $\theta=\omega$ is

$$G(\omega) = \frac{1}{2}\boldsymbol{k}'^{\,\mathrm{T}}\boldsymbol{L}_\omega^{-1}\boldsymbol{k}' \tag{6.3}$$

where

$$\boldsymbol{L}_{\omega}^{-1} = \boldsymbol{\Omega}(\omega)\boldsymbol{L}^{-1}\boldsymbol{\Omega}^{\mathrm{T}}(\omega)$$

$$\boldsymbol{k}' = \boldsymbol{c}\boldsymbol{k} + \sqrt{a}\boldsymbol{b}\boldsymbol{T} + a\boldsymbol{h}\boldsymbol{g} \tag{6.4}$$

From Eqs. (6.3) and (6.4)

$$G(\omega) = \frac{1}{2}\boldsymbol{k}^{\mathrm{T}}\boldsymbol{c}^{\mathrm{T}}\boldsymbol{L}_{\omega}^{-1}\left(\boldsymbol{c}\boldsymbol{k} + 2\sqrt{a}\boldsymbol{b}\boldsymbol{T} + 2a\boldsymbol{h}\boldsymbol{g}\right) + \frac{a}{2}\boldsymbol{T}^{\mathrm{T}}\boldsymbol{b}^{\mathrm{T}}\boldsymbol{L}_{\omega}^{-1}\boldsymbol{b}\boldsymbol{T} \tag{6.5}$$

The ratio of the two energy release rates is obtained from Eqs. (6.1) and (6.5) as

$$\frac{G(\omega)}{G_0} = \frac{\boldsymbol{n}^{\mathrm{T}}\boldsymbol{c}^{\mathrm{T}}\boldsymbol{L}_{\omega}^{-1}(\boldsymbol{c}\boldsymbol{n} + 2\boldsymbol{b}\boldsymbol{\beta} + 2\boldsymbol{h}\boldsymbol{\alpha}) + \boldsymbol{\beta}^{\mathrm{T}}\boldsymbol{b}^{\mathrm{T}}\boldsymbol{L}_{\omega}^{-1}\boldsymbol{b}\boldsymbol{\beta}}{\boldsymbol{n}^{\mathrm{T}}\boldsymbol{L}^{-1}\boldsymbol{n}} \tag{6.6}$$

where

$$\boldsymbol{\beta} = \frac{\boldsymbol{T}\sqrt{a}}{|\boldsymbol{k}|} = \left[\beta_1, 0, \beta_3\right]^{\mathrm{T}}, \qquad \boldsymbol{\alpha} = \frac{a\boldsymbol{g}}{|\boldsymbol{k}|} = [\alpha_1, \alpha_2, \alpha_3]^{\mathrm{T}}.$$

The fracture criterion based on energy release rate may be stated as follows: the kinked crack will propagate along the direction $\theta = \omega$ if

$$G(\omega) = G_c\left(\omega, \psi', \phi'\right) \tag{6.7}$$

Here $G(\omega)$ is the energy release rate which may be calculated from Eq. (6.5), G_c is the experimentally-determined fracture toughness which depends on the kink angle ω and the loading phase angles, ψ', and ϕ' of $\boldsymbol{k}'$.

If crack is kinked at $\theta = \omega$, then it raises a critical question: Whether the kinked crack will tend to arrest or grow further to damage the structure. Following the energy release rate fracture criterion, the stability conditions of the kinked crack may be stated as

$$\frac{\partial G(\omega)}{\partial a} < 0, \quad \text{kinked crack is stable}$$

$$\frac{\partial G(\omega)}{\partial a} > 0, \quad \text{kinked crack is unstable} \tag{6.8}$$

This means that the kinked crack is stable if $G(\omega)$ decreases with increases a, and the kinked crack is unstable if $G(\omega)$ increases as the crack grows (see He and Hutchinson, 1989). The dual condition of Eqs. (6.7) and (6.8) determines the kinking stability. From Eq. (6.5)

$$\frac{\partial G(\omega)}{\partial a} = \frac{|\boldsymbol{k}|^2}{2a}\left[\boldsymbol{n}^{\mathrm{T}}\boldsymbol{c}^{\mathrm{T}}\boldsymbol{L}_{\omega}^{-1}(\boldsymbol{b}\boldsymbol{\beta} + 2\boldsymbol{h}\boldsymbol{\alpha}) + \boldsymbol{\beta}^{\mathrm{T}}\boldsymbol{b}^{\mathrm{T}}\boldsymbol{L}_{\omega}^{-1}\boldsymbol{b}\boldsymbol{\beta} + O(a^{3/2})\right] \tag{6.9}$$

Eq. (6.9) may be written in more useful form as

$$\frac{\partial G(\omega)}{\partial a} = \frac{|\boldsymbol{k}|^2}{2l}\left[\boldsymbol{n}^{\mathrm{T}}\boldsymbol{c}^{\mathrm{T}}\boldsymbol{L}_{\omega}^{-1}\left(\frac{\boldsymbol{b}\tilde{\boldsymbol{\beta}}}{\sqrt{a/l}} + 2\boldsymbol{h}\tilde{\boldsymbol{\alpha}}\right) + \tilde{\boldsymbol{\beta}}^{\mathrm{T}}\boldsymbol{b}^{\mathrm{T}}\boldsymbol{L}_{\omega}^{-1}\boldsymbol{b}\tilde{\boldsymbol{\beta}} + O\left(\sqrt{a/l}\right)\right] \tag{6.10}$$

where

$$\tilde{\boldsymbol{\beta}} = \sqrt{l}\boldsymbol{T}/|\boldsymbol{k}| = \left[\tilde{\beta}_1, 0, \tilde{\beta}_3\right]^{\mathrm{T}}, \quad \tilde{\boldsymbol{\alpha}} = l\boldsymbol{g}/|\boldsymbol{k}| = [\tilde{\alpha}_1, \tilde{\alpha}_2, \tilde{\alpha}_3]^{\mathrm{T}}, \tag{6.11}$$

l is a characteristic length of the cracked body. For example, l can be taken as the main crack length; $\tilde{\boldsymbol{\beta}}$ and $\tilde{\boldsymbol{\alpha}}$ are nondimensional constant vectors which depend on the geometry of the cracked body and the type of loading and are independent of the kinking length a and the loading magnitude. For mode-I loading, $\tilde{\beta}_1$ is usually called a biaxial parameter. Then stability condition of the kinked crack (6.8) with (6.10) becomes

$$\boldsymbol{n}^{\mathrm{T}}\boldsymbol{c}^{\mathrm{T}}\boldsymbol{L}_{\omega}^{-1}\left(\frac{\boldsymbol{b}\tilde{\boldsymbol{\beta}}}{\sqrt{a/l}} + 2\boldsymbol{h}\tilde{\boldsymbol{\alpha}}\right) + \tilde{\boldsymbol{\beta}}^{\mathrm{T}}\boldsymbol{b}^{\mathrm{T}}\boldsymbol{L}_{\omega}^{-1}\boldsymbol{b}\tilde{\boldsymbol{\beta}} < 0 \tag{6.12}$$

It is worth noting that the stability condition is independent of the loading magnitude. This is one of the motives why $\boldsymbol{b}$ and $\boldsymbol{h}$ are calculated by this paper. $\tilde{\boldsymbol{\beta}}$ and $\tilde{\boldsymbol{\alpha}}$ (or $\boldsymbol{T}$ and $\boldsymbol{g}$) can be determined by using path-independent integrals (see authors' paper). Since $a/l \ll 1$, it follows from Eq. (6.12) that

$$\boldsymbol{n}^{\mathrm{T}}\boldsymbol{c}^{\mathrm{T}}\boldsymbol{L}_{\omega}^{-1}\boldsymbol{b}\tilde{\boldsymbol{\beta}} < 0 \quad \text{if } \boldsymbol{b}\tilde{\boldsymbol{\beta}} = O(1) \tag{6.13}$$

$$\boldsymbol{n}^{\mathrm{T}}\boldsymbol{c}^{\mathrm{T}}\boldsymbol{L}_{\omega}^{-1}\boldsymbol{h}\tilde{\boldsymbol{\alpha}} < 0 \quad \text{if } \boldsymbol{b}\tilde{\boldsymbol{\beta}} = o\left(\sqrt{a/l}\right) \tag{6.14}$$

For other cases, $\boldsymbol{b}\tilde{\boldsymbol{\beta}} = O(\sqrt{a/l})$, Eq. (6.12) has to be used. Eq. (6.13) covers many cases. However, note that

$\boldsymbol{b} = 0$ at $\omega = 0$

$\boldsymbol{b} = O(\omega)$ at $\omega \ll 1$

$\tilde{\boldsymbol{\beta}} \approx 0$ when $\boldsymbol{T} \approx 0$

In these cases, the stability condition is given by Eq. (6.14) or (6.12). Eqs. (6.12)–(6.14) can be applied to any kinked angle ω if the kinked crack tip is open. If Eq. (6.13) or Eq. (6.14) can be applied, the stability condition is independent of a/l.

7. Stress intensity factors, *T*-stresses and energy release rate at the kinked tip in monoclinic material with symmetry plane at $x_3 = 0$

For general anisotropic materials, all three displacement components are coupled and depend on x_1 and x_2 only. The components, $q_1(t)$, $q_2(t)$, and $q_3(t)$ of dislocation density $\boldsymbol{q}(t)$, have to be considered simultaneously in the integral equation (3.19). However, for monoclinic materials with symmetry plane at $x_3 = 0$, the in-plane deformations are decoupled from the anti-plane deformation, we may consider the in-plane deformation and the antiplane deformation, respectively. In this case, explicit expressions of $\boldsymbol{B}, \boldsymbol{B}^{-1}$, and $\boldsymbol{L}^{-1}$ are given by

$$\boldsymbol{B}=\begin{bmatrix}-p_1 & -p_2 & 0\\ 1 & 1 & 0\\ 0 & 0 & -1\end{bmatrix},\qquad \boldsymbol{B}^{-1}=\frac{1}{p_1-p_2}\begin{bmatrix}-1 & -p_2 & 0\\ 1 & p_1 & 0\\ 0 & 0 & p_2-p_1\end{bmatrix} \tag{7.1}$$

$$\boldsymbol{L}^{-1}=s'_{11}\begin{bmatrix}\mathrm{Im}(p_1+p_2) & \mathrm{Im}(p_1p_2) & 0\\ \mathrm{Im}(p_1p_2) & \mathrm{Im}\left[p_1p_2(\bar{p}_1+\bar{p}_2)\right] & 0\\ 0 & 0 & \left(\mu s'_{11}\right)^{-1}\end{bmatrix} \tag{7.2}$$

where

$$\mu=\left(s'_{44}s'_{55}-s'^{2}_{45}\right)^{-1/2} \tag{7.3}$$

p_1 and p_2 are the roots of

$$s'_{11}p^4-2s'_{16}p^3+\left(2s'_{12}+s'_{66}\right)p^2-2s'_{26}p+s'_{22}=0 \tag{7.4}$$

with positive imaginary part; p_3 is the root of

$$s'_{55}p^2-2s'_{45}p+s'_{44}=0,\quad \mathrm{Im}[p_3]>0. \tag{7.5}$$

With these expressions, the system of integral equations (3.19) reduces to the following a pair of integral equations (7.6) for in-plane deformation and an integral equation (7.7) for anti-plane deformation:

$$\begin{aligned}&\int_{-1}^{1}\left\{\frac{\mathbf{I}}{t-x}+\frac{1}{2}\frac{\mathbf{I}}{1+x+\sqrt{(1+x)(1+t)}}+\frac{1}{2}\sum_{\beta=1}^{2}\mathrm{Re}\left[\boldsymbol{B}\langle\frac{1}{1+x+\sqrt{(1+x)(1+t)}\bar{\varsigma}_\beta/\varsigma}\rangle\boldsymbol{Y}_\beta\right]\right.\\ &\quad\left.\times\right\}\frac{\boldsymbol{q}(t)\,\mathrm{d}t}{(1+t)^s(1-t)^{1/2}}\\ &=\frac{1}{\sqrt{\pi(1+x)}}\mathrm{Re}\left[\boldsymbol{B}\langle\sqrt{\varsigma}\rangle\boldsymbol{B}^{-1}\right]\boldsymbol{k}-\sqrt{a}\boldsymbol{T}\sin\omega+a\sqrt{\frac{1+x}{\pi}}\mathrm{Re}\left[\boldsymbol{B}\langle\varsigma^{3/2}\rangle\boldsymbol{B}^{-1}\right]\boldsymbol{g}+O(a^2)\end{aligned} \tag{7.6}$$

$$\begin{aligned}&\int_{-1}^{1}\left\{\frac{1}{t-x}+\frac{1}{2}\frac{1}{1+x+\sqrt{(1+x)(1+t)}}+\frac{1}{2}\mathrm{Re}\left[\frac{1}{1+x+\sqrt{(1+x)(1+t)}\bar{\varsigma}_3/\varsigma_3}\right]\right\}\frac{q_3(t)\,\mathrm{d}t}{(1+t)^s(1-t)^{1/2}}\\ &=\frac{1}{\sqrt{\pi(1+x)}}\mathrm{Re}\left(\sqrt{\varsigma_3}\right)k_3-\sqrt{a}T_3\sin\omega+a\sqrt{\frac{1+x}{\pi}}\mathrm{Re}\left(\varsigma_3^{3/2}\right)g_3\end{aligned} \tag{7.7}$$

where $\boldsymbol{q}=[q_1,q_2]^{\mathrm{T}}$, $\boldsymbol{k}=[k_2,k_1]^{\mathrm{T}}$, $\boldsymbol{g}=[g_2,g_1]^{\mathrm{T}}$

$$\boldsymbol{Y}_\beta=\boldsymbol{B}^{-1}\bar{\boldsymbol{B}}\mathbf{I}_\beta\bar{\boldsymbol{B}}^{-1},\quad \beta=1,2 \tag{7.8}$$

$\mathbf{B}$, $\boldsymbol{Y}_\beta$, $\mathbf{I}$, $\mathbf{I}_\beta$ are 2×2 matrices obtained by deleting the third row and the third column in the corresponding matrices (3.7). It is clear that q_1, q_2 are independent of k_3 and T_3, and q_3 is independent

of k_1, k_2, T_1, g_1, g_2. In this case,

$$c_{23} = c_{13} = c_{32} = c_{31} = 0, \qquad b_{31} = b_{23} = b_{13} = 0$$

$$h_{23} = h_{13} = h_{32} = h_{31} = 0, \qquad d_{13} = d_{32} = d_{31} = 0$$

$$e_{13} = e_{31} = 0 \tag{7.9}$$

Therefore, the expressions of $\boldsymbol{k}'$ in Eq. (4.6) and $\boldsymbol{T}'$ in Eq. (5.12) can be simplified.

7.1. In-plane deformation

The 3×3 matrices $\boldsymbol{c}$, $\boldsymbol{h}$, defined before reduce to 2×2 matrices; the matrices $\boldsymbol{b}$ and $\boldsymbol{d}$ reduce to two-dimensional column and row vectors respectively; $\boldsymbol{e}$ reduces to a scalar. Thus

$$\begin{bmatrix} k_2' \\ k_1' \end{bmatrix} = \begin{bmatrix} c_{22} & c_{21} \\ c_{12} & c_{11} \end{bmatrix} \begin{bmatrix} k_2 \\ k_1 \end{bmatrix} + \sqrt{a} T_1 \begin{bmatrix} b_2 \\ b_1 \end{bmatrix} + a \begin{bmatrix} h_{22} & h_{21} \\ h_{12} & h_{11} \end{bmatrix} \begin{bmatrix} g_2 \\ g_1 \end{bmatrix} \tag{7.10}$$

$$T_1' = \frac{d_2 k_2 + d_1 k_1}{\sqrt{a}} + e T_1 \tag{7.11}$$

or

$$\boldsymbol{k}' = \boldsymbol{c}\boldsymbol{k} + \sqrt{a} T_1 \boldsymbol{b} + a \boldsymbol{h}\boldsymbol{g} \tag{7.12}$$

$$T_1' = \frac{\boldsymbol{d}^{\mathrm{T}} \boldsymbol{k}}{\sqrt{a}} + e T_1 \tag{7.13}$$

where, for simplicity, we have introduced the notations:

$$\boldsymbol{b} = [b_2, b_1]^{\mathrm{T}}, \quad b_2 = b_{21}, \quad b_1 = b_{11},$$

$$\boldsymbol{d} = [d_2, d_1]^{\mathrm{T}}, \quad d_2 = d_{12}, \quad d_1 = d_{11},$$

$$e = e_{11}.$$

The energy release rates for the in-plane deformation lead to

$$G(\omega) = \frac{1}{2} \boldsymbol{k}^{\mathrm{T}} \boldsymbol{c}^{\mathrm{T}} \boldsymbol{L}_{\omega}^{-1} \left(\boldsymbol{c}\, \boldsymbol{k} + 2\sqrt{a} T_1 \boldsymbol{b} + 2a \boldsymbol{h}\, \boldsymbol{g} \right) + \frac{a}{2} T_1^2 \boldsymbol{b}^{\mathrm{T}} \boldsymbol{L}_{\omega}^{-1} \boldsymbol{b} \tag{7.14}$$

$$G_0 = G(\omega)|_{\substack{\omega=0 \\ a \to 0}} = \frac{|\boldsymbol{k}|^2}{2} \boldsymbol{n}^{\mathrm{T}} \boldsymbol{L}^{-1} \boldsymbol{n} \tag{7.15}$$

and the ratio

$$\frac{G(\omega)}{G_0} = \left[\boldsymbol{n}^{\mathrm{T}} \boldsymbol{c}^{\mathrm{T}} \boldsymbol{L}_{\omega}^{-1} (\boldsymbol{c}\, \boldsymbol{n} + 2\beta \boldsymbol{b} + 2\boldsymbol{h}\boldsymbol{\alpha}) + \beta^2 \boldsymbol{b}^{\mathrm{T}} \boldsymbol{L}_{\omega}^{-1} \boldsymbol{b} \right] / (\boldsymbol{n}^{\mathrm{T}} \boldsymbol{L}^{-1} \boldsymbol{n}) \tag{7.16}$$

where $\boldsymbol{n}=[\sin\psi, \cos\psi]^{\mathrm{T}}$, $\tan\psi = k_2/k_1$, $|\boldsymbol{k}| = \sqrt{k_1^2 + k_2^2}$. In this case, β_{3x1} and α_{3x1} defined before reduces to a scalar and a two-dimensional vector given by

$$\beta = \frac{\sqrt{a}T_1}{|\boldsymbol{k}|}, \qquad \boldsymbol{\alpha} = \frac{a\boldsymbol{g}}{|\boldsymbol{k}|} = [\alpha_1, \alpha_2]^{\mathrm{T}}$$

The expressions are also valid for degenerated materials. For isotropic materials,

$$\boldsymbol{L}^{-1} = \boldsymbol{L}_{\omega}^{-1} = \frac{2(1-\nu^2)}{E}\mathbf{I}$$

Therefore, we have

$$G(\omega) = \frac{1-\nu^2}{E}\left[\boldsymbol{k}^{\mathrm{T}}\boldsymbol{c}^{\mathrm{T}}\left(\boldsymbol{c}\boldsymbol{k} + 2\sqrt{a}T_1\boldsymbol{b} + 2a\boldsymbol{h}\boldsymbol{g}\right) + aT_1^2\boldsymbol{b}^{\mathrm{T}}\boldsymbol{b}\right] \tag{7.17}$$

$$\frac{G(\omega)}{G_0} = \boldsymbol{n}^{\mathrm{T}}\boldsymbol{c}^{\mathrm{T}}(\boldsymbol{c}\boldsymbol{n} + 2\beta\boldsymbol{b} + 2\boldsymbol{h}\boldsymbol{\alpha}) + \beta^2\boldsymbol{b}^{\mathrm{T}}\boldsymbol{b} \tag{7.18}$$

In the absence of k_3, for in-plane deformation of monoclinic materials, the criterion (6.7) becomes

$$G(\omega) = G_c(\omega, \psi') \tag{7.19}$$

where $\psi' = \tan^{-1}(k_2'/k_1')$ is the phase angle of $\boldsymbol{k}'$ and Eq. (6.10) yields

$$\frac{\partial G(\omega)}{\partial a} = \frac{|\boldsymbol{k}|^2}{2l}\left[\boldsymbol{n}^{\mathrm{T}}\boldsymbol{c}^{\mathrm{T}}\boldsymbol{L}_{\omega}^{-1}\left(\frac{\boldsymbol{b}\tilde{\beta}}{\sqrt{a/l}} + 2\boldsymbol{h}\tilde{\boldsymbol{\alpha}}\right) + \tilde{\beta}^2\boldsymbol{b}^{\mathrm{T}}\boldsymbol{L}_{\omega}^{-1}\boldsymbol{b} + O\left(\sqrt{a/l}\right)\right] \tag{7.20}$$

The stability condition in Eq. (6.12) becomes

$$\boldsymbol{n}^{\mathrm{T}}\boldsymbol{c}^{\mathrm{T}}\boldsymbol{L}_{\omega}^{-1}\left(\frac{\boldsymbol{b}\tilde{\beta}}{\sqrt{a/l}} + 2\boldsymbol{h}\tilde{\boldsymbol{\alpha}}\right) + \tilde{\beta}^2\boldsymbol{b}^{\mathrm{T}}\boldsymbol{L}_{\omega}^{-1}\boldsymbol{b} < 0 \tag{7.21}$$

Here, $\tilde{\beta}$ and $\tilde{\boldsymbol{\alpha}}$ are given by $\tilde{\beta} = \sqrt{l}T_1/|\boldsymbol{k}|$, $\tilde{\boldsymbol{\alpha}} = l\boldsymbol{g}/|\boldsymbol{k}| = [\tilde{\alpha}_1, \tilde{\alpha}_2]^{\mathrm{T}}$.

Eq. (7.21) can be simplified into

$$\boldsymbol{n}^{\mathrm{T}}\boldsymbol{c}^{\mathrm{T}}\boldsymbol{L}_{\omega}^{-1}\boldsymbol{b}\tilde{\beta} < 0, \quad \text{if } \boldsymbol{b}\tilde{\beta} = O(1) \tag{7.22}$$

$$\boldsymbol{n}^{\mathrm{T}}\boldsymbol{c}^{\mathrm{T}}\boldsymbol{L}_{\omega}^{-1}\boldsymbol{h}\tilde{\boldsymbol{\alpha}} < 0, \quad \text{if } \boldsymbol{b}\tilde{\beta} = \boldsymbol{o}\left(\sqrt{a/l}\right) \tag{7.23}$$

For mode-I,

$$[c_{21}, c_{11}]^{\mathrm{T}}\boldsymbol{L}_{\omega}^{-1}\boldsymbol{b}\tilde{\beta} < 0, \quad \text{if } \boldsymbol{b}\tilde{\beta} = \boldsymbol{O}(1) \tag{7.24}$$

$$[c_{21}, c_{11}]^{\mathrm{T}}\boldsymbol{L}_{\omega}^{-1}[h_{21}, h_{11}]^{\mathrm{T}}\tilde{\alpha}_1 < 0, \quad \text{if } \boldsymbol{b}\tilde{\beta} = \boldsymbol{o}\left(\sqrt{a/l}\right) \tag{7.25}$$

For mode-II,

$$[c_{22}, c_{12}]^{\mathrm{T}}\boldsymbol{L}_{\omega}^{-1}\boldsymbol{b}\tilde{\beta} < 0, \quad \text{if } \boldsymbol{b}\tilde{\beta} = \boldsymbol{O}(1) \tag{7.26}$$

$$[c_{22}, c_{12}]^{\mathrm{T}}\boldsymbol{L}_{\omega}^{-1}[h_{22}, h_{12}]^{\mathrm{T}}\tilde{\alpha}_2 < 0, \quad \text{if } \boldsymbol{b}\tilde{\beta} = \boldsymbol{o}\left(\sqrt{a/l}\right) \tag{7.27}$$

For orthotropic materials, when the main crack line coincides with one material principal axis, it is easy to prove that the following relations hold:

$$c_{ij}(-\omega) = (-1)^{i+j}c_{ij}(\omega), \quad b_i(-\omega) = (-1)^{i+1}b_i(\omega),$$

$$h_{ij}(-\omega) = (-1)^{i+j}h_{ij}(\omega), \quad d_i(-\omega) = (-1)^{i+1}d_i(\omega), \quad e(-\omega) = e(\omega) \tag{7.28}$$

7.2. Anti-plane deformation

All matrices defined reduce to scalars. Therefore

$$k_3' = c_3k_3 + \sqrt{a}b_3T_3 + ah_3g_3 \tag{7.29}$$

$$T_3' = \frac{d_3k_3}{\sqrt{a}} + e_3T_3 + O(a) \tag{7.30}$$

where the following notations are used:

$$c_3 = c_{33}, \quad b_3 = b_{33}, \quad h_3 = h_{33}, \quad d_3 = d_{33}, \quad e_3 = e_{33}.$$

The energy release rates and its ratio for antiplane deformation are

$$G_3(\omega) = \frac{c_3k_3}{2\mu}\left(c_3k_3 + 2\sqrt{a}T_3b_3 + 2ah_3g_3\right) + \frac{a}{2\mu}T_3^2b_3^2 \tag{7.31}$$

$$G_{3,0} = G_3(\omega)|_{\substack{\omega=0\\ a\to 0}} = \frac{k_3^2}{2\mu} \tag{7.32}$$

$$\frac{G_3(\omega)}{G_{3,0}} = c_3\left(c_3 + 2\beta_3b_3 + 2\alpha_3h_3\right) + \beta_3^2b_3^2 \tag{7.33}$$

Here, for convenience, β_3 and α_3 are redefined as $\beta_3 = \sqrt{a}T_3/k_3$. $\alpha_3 = ag_3/k_3$ and μ is invariant under in-plane rotation. In isotropic materials, μ is the shear modulus and the exact solution of c_3 has been found (Wu, 1978)

$$c_3 = \left(\frac{1-\omega/\pi}{1+\omega/\pi}\right)^{\omega/2\pi} \tag{7.34}$$

Note that the integral equation for $q_3(t)$, Eq. (7.7), can be applied to isotropic case directly. Numerical results from the integral equation are very close to the exact solution. For example, in the case of $\omega = \pi/2$, the relative difference is less than 0.07%.

For mode-III, from Eq. (7.31)

$$\frac{\partial G_3(\omega)}{\partial a} = \frac{G_0}{2\mu l}\left(\frac{\tilde{\beta}_3}{\sqrt{a/l}}c_3 b_3 + 2\tilde{\alpha}_3 c_3 h_3 + \tilde{\beta}_3^2 b_3^2\right) \tag{7.35}$$

where $\tilde{\beta}_3$ and $\tilde{\alpha}_3$ are given by

$$\tilde{\beta}_3 = \sqrt{l}T_3/k_3, \qquad \tilde{\alpha}_3 = lg_3/k_3 \tag{7.36}$$

The stability condition for kinked crack along $\theta = \omega$ under mode-III is

$$\frac{\tilde{\beta}_3}{\sqrt{a/l}}c_3 b_3 + 2\tilde{\alpha}_3 c_3 h_3 + \tilde{\beta}_3^2 b_3^2 < 0$$

which implies that

$$\tilde{\beta}_3 h_3 < 0 \quad \text{for } \tilde{\beta}_3 h_3 = O(1)$$

$$\tilde{\alpha}_3 h_3 < 0 \quad \text{for } \tilde{\beta}_3 h_3 = o\left(\sqrt{a/l}\right)$$

For orthotropic materials, when the main crack line coincides with one principal material axis, it is easy to show the following relations:

$$b_3(-\omega) = -b_3(\omega), \quad c_3(-\omega) = c_3(\omega), \quad h_3(-\omega) = h_3(\omega), \quad e_3(-\omega) = e_3(\omega) \tag{7.37}$$

8. Crack kinking at right angle from the main crack plane in orthotropic materials

For materials that possess a plane having lower fracture toughness than other planes, crack may be deflected towards such weak plane under favorable conditions. For example, the crack in a fiber reinforced composite material, it is usually expected to grow parallel to the stiffer material direction. It is interesting to describe the behavior of a parent crack in x_1-direction turning into x_2-direction in orthotropic materials. Here, we assume the coordinate axes (x_1, x_2, x_3) coincide with principal material axes. First consider the in-plane deformation. The Stroh eigenvalues, p_1 and p_2, are roots of

$$s'_{11}p^4 + \left(2s'_{12} + s'_{66}\right)p^2 + s'_{22} = 0 \tag{8.1}$$

or

$$\lambda p^4 + 2\rho\sqrt{\lambda}p^2 + 1 = 0$$

where

$$\lambda = \frac{s'_{11}}{s'_{22}}, \quad \rho = \frac{s'_{12} + s'_{66}/2}{\sqrt{s'_{11}s'_{22}}} \quad \text{and } \lambda > 0, \quad -1 < \rho < \infty. \tag{8.2}$$

These two parameters, λ and ρ, were introduced by Suo et al. (1991). It is obvious that the nondimensioanl coefficients, c_{ij}, b_i, h_{ij}, d_i, e, associated with in-plane deformation depend on λ and ρ for $\omega = \pi/2$. In order to extract explicitly the λ-dependence of these coefficients, the x_1-axis is scaled by

$$\zeta = \lambda^{1/4}x_1 \tag{8.3}$$

This scaling was first used by Suo et al. (1991) to get the explicit λ-dependence of c_{ij}, following a similar argument, the λ-dependence of b_i, h_{ij}, d_i, e, can be given as follows for $\omega = \pi/2$,

$$\begin{bmatrix} k_2' \\ k_1' \end{bmatrix} = \begin{bmatrix} \lambda^{1/8} c_{22}^* & \lambda^{-1/8} c_{21}^* \\ \lambda^{-1/8} c_{12}^* & \lambda^{-3/8} c_{11}^* \end{bmatrix} \begin{bmatrix} k_2 \\ k_1 \end{bmatrix} + \sqrt{a} T_1 \begin{bmatrix} \lambda^{1/4} b_2^* \\ b_1^* \end{bmatrix} + a \begin{bmatrix} \lambda^{-1/8} h_{22}^* & \lambda^{-3/8} h_{21}^* \\ \lambda^{-3/8} h_{12}^* & \lambda^{5/8} h_{11}^* \end{bmatrix} \begin{bmatrix} g_2 \\ g_1 \end{bmatrix} \tag{8.4}$$

$$T_1' = \frac{\lambda^{3/8} d_2^* k_2 + \lambda^{1/8} d_1^* k_1}{\sqrt{a}} + \lambda^{1/2} e^* T_1 \tag{8.5}$$

where all the quantities with superscript '$*$' which is function of ρ only can be calculated by solving the integral equations with $\lambda = s_{11}'/s_{22}' = 1$. c_{ij}^*, b_i^*, h_{ij}^*, d_i^*, and e^* are tabulated in Tables 1 and 2.

Table 1
Variation of coefficients as a function of ρ for orthotropic materials with kink angle $\omega = \pi/2$

ρ	c_{11}^*	c_{12}^*	c_{21}^*	c_{22}^*	b_1^*	b_2^*
0.1	0.3984	−1.0696	0.3699	−0.2215	1.8023	−0.2577
0.2	0.3948	−1.0860	0.3668	−0.2179	1.7958	−0.2486
0.3	0.3914	−1.1015	0.3639	−0.2147	1.7901	−0.2405
0.4	0.3882	−1.1162	0.3612	−0.2116	1.7850	−0.2332
0.5	0.3853	−1.1303	0.3586	−0.2088	1.7804	−0.2265
0.6	0.3824	−1.1437	0.3562	−0.2062	1.7763	−0.2205
0.7	0.3798	−1.1566	0.3539	−0.2038	1.7725	−0.2149
0.8	0.3772	−1.1690	0.3517	−0.2015	1.7690	−0.2098
0.9	0.3748	−1.1809	0.3496	−0.1993	1.7659	−0.2050
1.0	0.3725	−1.1925	0.3476	−0.1972	1.7629	−0.2006
1.1	0.3703	−1.2036	0.3457	−0.1953	1.7602	−0.1965
1.2	0.3681	−1.2144	0.3439	−0.1934	1.7577	−0.1926
1.3	0.3661	−1.2249	0.3421	−0.1917	1.7553	−0.1890
1.4	0.3641	−1.2350	0.3404	−0.1900	1.7531	−0.1856
1.5	0.3622	−1.2449	0.3388	−0.1884	1.7511	−0.1823
1.6	0.3604	−1.2545	0.3372	−0.1868	1.7491	−0.1793
1.7	0.3586	−1.2639	0.3357	−0.1853	1.7473	−0.1764
1.8	0.3569	−1.2730	0.3342	−0.1839	1.7456	−0.1736
1.9	0.3553	−1.2820	0.3328	−0.1825	1.7439	−0.1710
2.0	0.3536	−1.2907	0.3314	−0.1812	1.7424	−0.1685
2.5	0.3463	−1.3315	0.3251	−0.1753	1.7357	−0.1575
3.0	0.3398	−1.3685	0.3195	−0.1702	1.7303	−0.1486
3.5	0.3341	−1.4025	0.3145	−0.1658	1.7259	−0.1410
4.0	0.3289	−1.4339	0.3100	−0.1618	1.7222	−0.1346
4.5	0.3242	−1.4632	0.3059	−0.1584	1.7191	−0.1290
5.0	0.3199	−1.4908	0.3022	−0.1552	1.7164	−0.1240
5.5	0.3159	−1.5168	0.2987	−0.1523	1.7140	−0.1196
6.0	0.3122	−1.5414	0.2955	−0.1497	1.7119	−0.1157
6.5	0.3088	−1.5648	0.2925	−0.1473	1.7100	−0.1121
7.0	0.3056	−1.5872	0.2897	−0.1451	1.7083	−0.1089
7.5	0.3026	−1.6086	0.2870	−0.1430	1.7068	−0.1059
8.0	0.2997	−1.6291	0.2845	−0.1410	1.7054	−0.1032
8.5	0.2970	−1.6488	0.2821	−0.1392	1.7042	−0.1007
9.0	0.2945	−1.6678	0.2799	−0.1375	1.7030	−0.0984
9.5	0.2920	−1.6862	0.2778	−0.1359	1.7019	−0.0962
10.0	0.2897	−1.7039	0.2757	−0.1343	1.7009	−0.0941

Comparing the values of c_{ij}^{*} provided in this paper with those of Suo et al. (1991) shows that the relative differences are very minor. The values for isotropic materials, $\rho = 1$, are listed in the Tables 1 and 2. The values of c_{ij} and b_i given in this paper are almost identical to those given by Melin (1994) and Khrapkov (1998), respectively. Because

$$\boldsymbol{L}^{-1} = s'_{11}\lambda^{-3/4}\sqrt{2(1+\rho)}\mathrm{diag}\left[\sqrt{\lambda}, 1\right] \tag{8.6}$$

$$\boldsymbol{L}_{90}^{-1} = s'_{11}\lambda^{-3/4}\sqrt{2(1+\rho)}\mathrm{diag}\left[1, \sqrt{\lambda}\right] \tag{8.7}$$

the energy release rate ratio from Eq. (7.16) leads to

Table 2
Variation of coefficients as a function of ρ for orthotropic materials with kink angle $\omega = \pi/2$

ρ	h_{11}^{*}	h_{12}^{*}	h_{21}^{*}	h_{22}^{*}	d_1^{*}	d_2^{*}	e^{*}
0.1	1.0010	1.1865	0.3166	−1.1650	0.2154	0.0891	−0.7696
0.2	1.0170	1.2800	0.3135	−1.1845	0.2224	0.0928	−0.7714
0.3	1.0322	1.3713	0.3107	−1.2030	0.2289	0.0964	−0.7730
0.4	1.0466	1.4606	0.3080	−1.2206	0.2351	0.0997	−0.7745
0.5	1.0603	1.5481	0.3055	−1.2373	0.2409	0.1029	−0.7758
0.6	1.0735	1.6339	0.3032	−1.2533	0.2465	0.1060	−0.7771
0.7	1.0861	1.7183	0.3010	−1.2686	0.2518	0.1089	−0.7783
0.8	1.0982	1.8012	0.2988	−1.2833	0.2569	0.1117	−0.7794
0.9	1.1099	1.8829	0.2968	−1.2974	0.2618	0.1145	−0.7805
1.0	1.1212	1.9634	0.2949	−1.3111	0.2669	0.1178	−0.7812
1.1	1.1322	2.0428	0.2931	−1.3243	0.2711	0.1196	−0.7824
1.2	1.1427	2.1212	0.2914	−1.3371	0.2754	0.1221	−0.7833
1.3	1.1530	2.1986	0.2897	−1.3494	0.2797	0.1245	−0.7842
1.4	1.1630	2.2751	0.2881	−1.3614	0.2838	0.1268	−0.7850
1.5	1.1727	2.3507	0.2865	−1.3731	0.2877	0.1291	−0.7857
1.6	1.1821	2.4254	0.2850	−1.3845	0.2916	0.1313	−0.7865
1.7	1.1913	2.4995	0.2836	−1.3955	0.2953	0.1335	−0.7872
1.8	1.2003	2.5727	0.2822	−1.4063	0.2990	0.1355	−0.7879
1.9	1.2090	2.6453	0.2809	−1.4168	0.3025	0.1376	−0.7885
2.0	1.2175	2.7172	0.2796	−1.4270	0.3059	0.1396	−0.7891
2.5	1.2576	3.0675	0.2736	−1.4751	0.3220	0.1489	−0.7919
3.0	1.2939	3.4046	0.2684	−1.5185	0.3364	0.1574	−0.7943
3.5	1.3272	3.7308	0.2638	−1.5582	0.3495	0.1651	−0.7963
4.0	1.3581	4.0474	0.2597	−1.5950	0.3615	0.1723	−0.7981
4.5	1.3868	4.3559	0.2559	−1.6293	0.3726	0.1790	−0.7997
5.0	1.4138	4.6571	0.2525	−1.6614	0.3830	0.1852	−0.8011
5.5	1.4393	4.9518	0.2493	−1.6917	0.3927	0.1911	−0.8023
6.0	1.4634	5.2407	0.2464	−1.7203	0.4019	0.1967	−0.8035
6.5	1.4863	5.5242	0.2437	−1.7476	0.4106	0.2019	−0.8045
7.0	1.5082	5.8029	0.2411	−1.7736	0.4188	0.2070	−0.8055
7.5	1.5292	6.0772	0.2387	−1.7984	0.4267	0.2118	−0.8064
8.0	1.5493	6.3473	0.2365	−1.8222	0.4342	0.2164	−0.8072
8.5	1.5686	6.6136	0.2343	−1.8451	0.4414	0.2208	−0.8080
9.0	1.5872	6.8763	0.2323	−1.8671	0.4483	0.2250	−0.8087
9.5	1.6051	7.1357	0.2304	−1.8884	0.4549	0.2291	−0.8094
10.0	1.6225	7.3919	0.2286	−1.9089	0.4613	0.2331	−0.8100

$$\frac{G_{90}}{G_0}=\Big\{\lambda^{1/4}\big(c_{22}^{*2}+c_{12}^{*2}\big)\sin^2\psi+\big(c_{22}^{*}c_{21}^{*}+c_{11}^{*}c_{12}^{*}\big)\sin 2\psi+\lambda^{-1/4}\big(c_{11}^{*2}+c_{21}^{*2}\big)\cos^2\psi+2\beta\Big[\lambda^{3/8}\big(b_2^{*}c_{22}^{*}+b_1^{*}c_{12}^{*}\big)\sin\psi+\lambda^{1/8}\big(b_2^{*}c_{21}^{*}+b_1^{*}c_{11}^{*}\big)\cos\psi\Big]+2\big(c_{22}^{*}h_{22}^{*}+c_{12}^{*}h_{12}^{*}\big)\tilde{\alpha}_2\sin\psi+2\lambda^{-1/4}\Big[\big(c_{22}^{*}h_{21}^{*}+c_{12}^{*}h_{11}^{*}\big)\tilde{\alpha}_1\sin\psi+\big(c_{21}^{*}h_{22}^{*}+c_{11}^{*}h_{12}^{*}\big)\tilde{\alpha}_2\cos\psi\Big]+2\lambda^{-1/2}\big(c_{21}^{*}h_{21}^{*}+c_{11}^{*}h_{11}^{*}\big)\tilde{\alpha}_1\cos\psi+\beta^2\lambda^{1/2}\big(b_2^{*2}+b_1^{*2}\big)\Big\}\Big/\Big(\sqrt{\lambda}\sin^2\psi+\cos^2\psi\Big) \tag{8.8}$$

When the main crack is subjected to a predominantly mode-I loading, $k_1>0$, $k_2=0$, from Eq. (8.8)

$$\frac{G_{90}}{G_0}=\lambda^{-1/4}\big(c_{11}^{*2}+c_{21}^{*2}\big)+2\beta\lambda^{1/8}\big(b_2^{*}c_{21}^{*}+b_1^{*}c_{11}^{*}\big)+2\alpha_1\lambda^{-1/2}\big(c_{21}^{*}h_{21}^{*}+c_{11}^{*}h_{11}^{*}\big)+\beta^2\lambda^{1/2}\big(b_2^{*2}+b_1^{*2}\big) \tag{8.9}$$

The first terms in Eqs. (8.8) and (8.9) representing the ratio when $\beta=0$ was given by Hutchinson and Suo (1992). From Eq. (7.20), we have

$$\frac{\partial G_{90}}{\partial a}=\frac{|\boldsymbol{k}|^2}{2l}\left[\boldsymbol{n}^{\mathrm{T}}\boldsymbol{c}^{\mathrm{T}}\boldsymbol{L}_{\omega}^{-1}\left(\frac{\boldsymbol{b}\tilde{\beta}}{\sqrt{a/l}}+2\boldsymbol{h}\tilde{\boldsymbol{\alpha}}\right)+\tilde{\beta}^2\boldsymbol{b}^{\mathrm{T}}\boldsymbol{L}_{\omega}^{-1}\boldsymbol{b}\right]\Bigg|_{\omega=90} \tag{8.10}$$

which can be expanded as

$$\begin{aligned}\frac{\partial G_{90}}{\partial a}=\frac{|\boldsymbol{k}|^2}{2l}s_{11}'\lambda^{-3/4}\sqrt{2(1+\rho)}\Big\{&\frac{\tilde{\beta}}{\sqrt{a/l}}\Big[\lambda^{3/8}\big(b_2^{*}c_{22}^{*}+b_1^{*}c_{12}^{*}\big)\sin\psi+\lambda^{1/8}\big(b_2^{*}c_{21}^{*}+b_1^{*}c_{11}^{*}\big)\cos\psi\Big]\\&+2\big(c_{22}^{*}h_{22}^{*}+c_{12}^{*}h_{12}^{*}\big)\tilde{\alpha}_2\sin\psi\\&+2\lambda^{-1/4}\Big[\big(c_{22}^{*}h_{21}^{*}+c_{12}^{*}h_{11}^{*}\big)\tilde{\alpha}_1\sin\psi+\big(c_{21}^{*}h_{22}^{*}+c_{11}^{*}h_{12}^{*}\big)\tilde{\alpha}_2\cos\psi\Big]\\&+2\lambda^{-1/2}\big(c_{21}^{*}h_{21}^{*}+c_{11}^{*}h_{11}^{*}\big)\tilde{\alpha}_1\cos\psi+\tilde{\beta}^2\lambda^{1/2}\big(b_2^{*2}+b_1^{*2}\big)\Big\}\end{aligned} \tag{8.11}$$

The stability condition (7.21) becomes

$$\left[\boldsymbol{n}^{\mathrm{T}}\boldsymbol{c}^{\mathrm{T}}\boldsymbol{L}_{\omega}^{-1}\left(\frac{\boldsymbol{b}\tilde{\beta}}{\sqrt{a/l}}+2\boldsymbol{h}\tilde{\boldsymbol{\alpha}}\right)+\tilde{\beta}^2\boldsymbol{b}^{\mathrm{T}}\boldsymbol{L}_{\omega}^{-1}\boldsymbol{b}\right]_{\omega=90}<0 \tag{8.12}$$

In the range of $0<\rho<10$, it can be proved from Tables 1 and 2 that all the coefficients of $\tilde{\beta}$, $\tilde{\alpha}_1$, $\tilde{\alpha}_2$ in Eq. (8.11) or (8.12) are non-negative if $\psi\leq 0$, and G_{90} decreases with ψ when $\psi>0$, in general. Therefore, for $\omega=90^\circ$, we consider $\psi\leq 0$. Eqs. (8.11) and (8.12) can be simplified in the following two cases:

$$\tilde{\beta}<0 \quad \text{if } \tilde{\beta}=O(1) \tag{8.13}$$

$$\tilde{\alpha}_1\Big[\lambda^{-1/4}\big(c_{22}^{*}h_{21}^{*}+c_{12}^{*}h_{11}^{*}\big)\sin\psi+\lambda^{-1/2}\big(c_{21}^{*}h_{21}^{*}+c_{11}^{*}h_{11}^{*}\big)\cos\psi\Big]$$

$$+\tilde{\alpha}_2\left[\left(c_{22}^*h_{22}^*+c_{12}^*h_{12}^*\right)\sin\psi+\lambda^{-1/4}\left(c_{21}^*h_{22}^*+c_{11}^*h_{12}^*\right)\cos\psi\right]<0 \quad \text{if } \tilde{\beta}=o\left(\sqrt{a/l}\right) \tag{8.14}$$

For mode-I, $\psi=0^\circ$

$$\tilde{\beta}<0 \quad \text{if } \tilde{\beta}=O(1)$$

$$\tilde{\alpha}_1<0 \quad \text{if } \tilde{\beta}=o\left(\sqrt{a/l}\right)$$

For mode-II, $\psi=-90^\circ$

$$\tilde{\beta}<0 \quad \text{if } \tilde{\beta}=O(1)$$

$$\tilde{\alpha}_2<0 \quad \text{if } \tilde{\beta}=o\left(\sqrt{a/l}\right)$$

Making a similar argument, if $\omega=-90^\circ$ is the possible kink direction, $\psi>0$ needs to be considered. The expressions of G_{-90} and $\frac{\partial G_{-90}}{\partial a}$ have the same forms as those in the case $\omega=90^\circ$, but the values of c_{ij}^* and h_{ij}^* should be taken at $\omega=-90^\circ$.

For anti-plane deformation,

$$p_3=i\sqrt{s'_{44}/s'_{55}} \quad \text{or} \quad p_3=i\lambda_3^{1/2} \tag{8.15}$$

where

$$\lambda_3=\frac{s'_{44}}{s'_{55}}>0. \tag{8.16}$$

For $\omega=\pi/2$, c_{33}^*, b_3^*, h_3^*, d_3^*, e_3^* are functions of λ_3 only. We scale the x_1-axis by

$$\zeta=\lambda_3^{-1/2}x_1 \tag{8.17}$$

Making similar arguments as that for in-plane deformation, the λ_3-dependence on k_3 and T_3 is given as

$$k'_3=\lambda_3^{1/4}c_3^*k_3+\sqrt{a}b_3^*T_3+a\lambda^{3/4}h_3^*g_3 \tag{8.18}$$

$$T'_3=\frac{\lambda_3^{-1/4}d_3^*k_3}{\sqrt{a}}+\lambda_3^{-1/2}e_3^*T_3 \tag{8.19}$$

where c_3^*, b_3^*, h_3^*, d_3^*, e_3^* are constants calculated from the corresponding integral equation, (7.7) with $\lambda_3=s'_{44}/s'_{55}=1$ and given by

$$c_3^*=0.7594, \quad b_3^*=-1.672, \quad h_3^*=-0.7312, \quad d_3^*=0.2334, \quad e_3^*=0.06423 \tag{8.20}$$

The energy release rate ratio is

$$\frac{G_{3,90}}{G_{3,0}}=\lambda_3^{1/2}c_3^{*2}+2\beta_3\lambda_3^{1/4}b_3^*c_3^*+2\alpha_3\lambda h_3^*c_3^*+\beta_3^2b_3^{*^2} \tag{8.21}$$

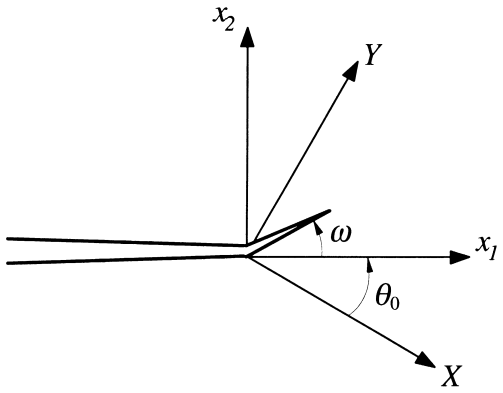

Fig. 2. Crack orientation and principal material axes for a kinked crack.

9. Numerical results and discussion

In order to provide some insights and better understanding of the role of anisotropy in kinking behavior, the following numerical results are limited to materials with orthotropic symmetry. Let X, Y, and Z be the principal material axes and x_1, x_2, and x_3 be the fixed coordinate axes. Assume x_3 is coincident with Z. The main crack shown in Fig. 2 is lying along $x_2 = 0$ and $x_1 < 0$ and the crack plane makes an angle θ_0 from the material X-axis. The angle θ_0 termed as crack orientation is considered to be positive if counterclockwise. Since the in-plane and anti-plane deformations are decoupled, they will be treated separately in this section.

First, we consider the in-plane deformation. Based on the previous analyses, the solutions, c_{ij}, b_i, h_{ij}, d_i, and e for crack kinking will depend on six reduced compliances, s'_{11}, s'_{12}, s'_{22}, s'_{16}, s'_{26}, and s'_{66} for an arbitrary crack orientation, θ_0. In order to reduce the material parameters in the solutions, we introduce two dimensionless parameters

$$\lambda = \frac{s'_{XX}}{s'_{YY}}, \qquad \rho = \frac{\left(2s'_{XY} + 1/G_{XY}\right)}{2\sqrt{s'_{XX}s'_{YY}}} \tag{9.1}$$

where s'_{XX}, s'_{YY}, and s'_{XY} are reduced compliances defined in the principal material coordinate system (X, Y, Z). Then the solutions will depend on three parameters, λ, ρ, and θ_0. To show the effect of the crack orientation on crack kinking, we assume $s'_{XX}/s'_{YY} > 1$ without loss of generality. This means that Y and X are along the stiffer and weaker principal material axes respectively. Thus, we can conclude that the solutions under general mixed-mode loading will depend on ω, λ, ρ, and θ_0. For a given material and θ_0, solutions for the coefficients c_{ij}, b_i, h_{ij}, d_i, e as a function of ω can be computed from the system of singular integral equations.

In observing crack kinking phenomenon for composites in laboratory experiments, the specimens are usually conducted along the principal material axes under symmetric pure mode-I loading. Since small

Fig. 3. (a) Variation of the stress intensity factors, k'_1, k'_2 and the energy release rate G at the kinked crack tip with the kink angle ω for various values of the T-stress parameter β for two materials. The main crack with orientation $\theta_0 = -5^\circ$ is subjected to mixed loading $\psi = 5^\circ$. (b) Variation of the stress intensity factors, k'_1, k'_2, at the kinked crack tip with the kink angle ω for different values of the T-stress parameter β for three materials. The main crack with orientation $\theta_0 = 90^\circ$ is subjected to mode-I loading $\psi = 0$.

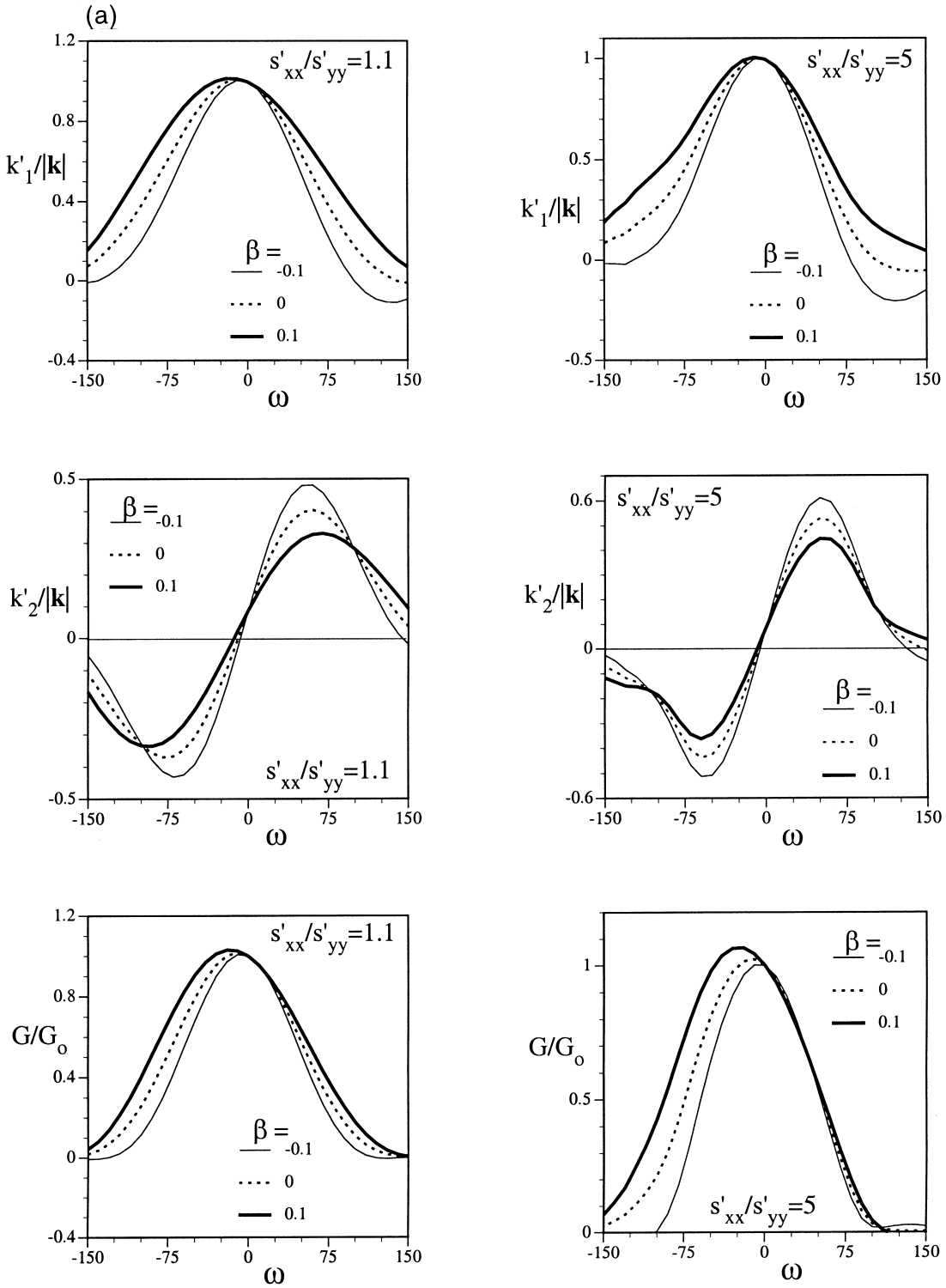

Fig. 3 (*continued*)

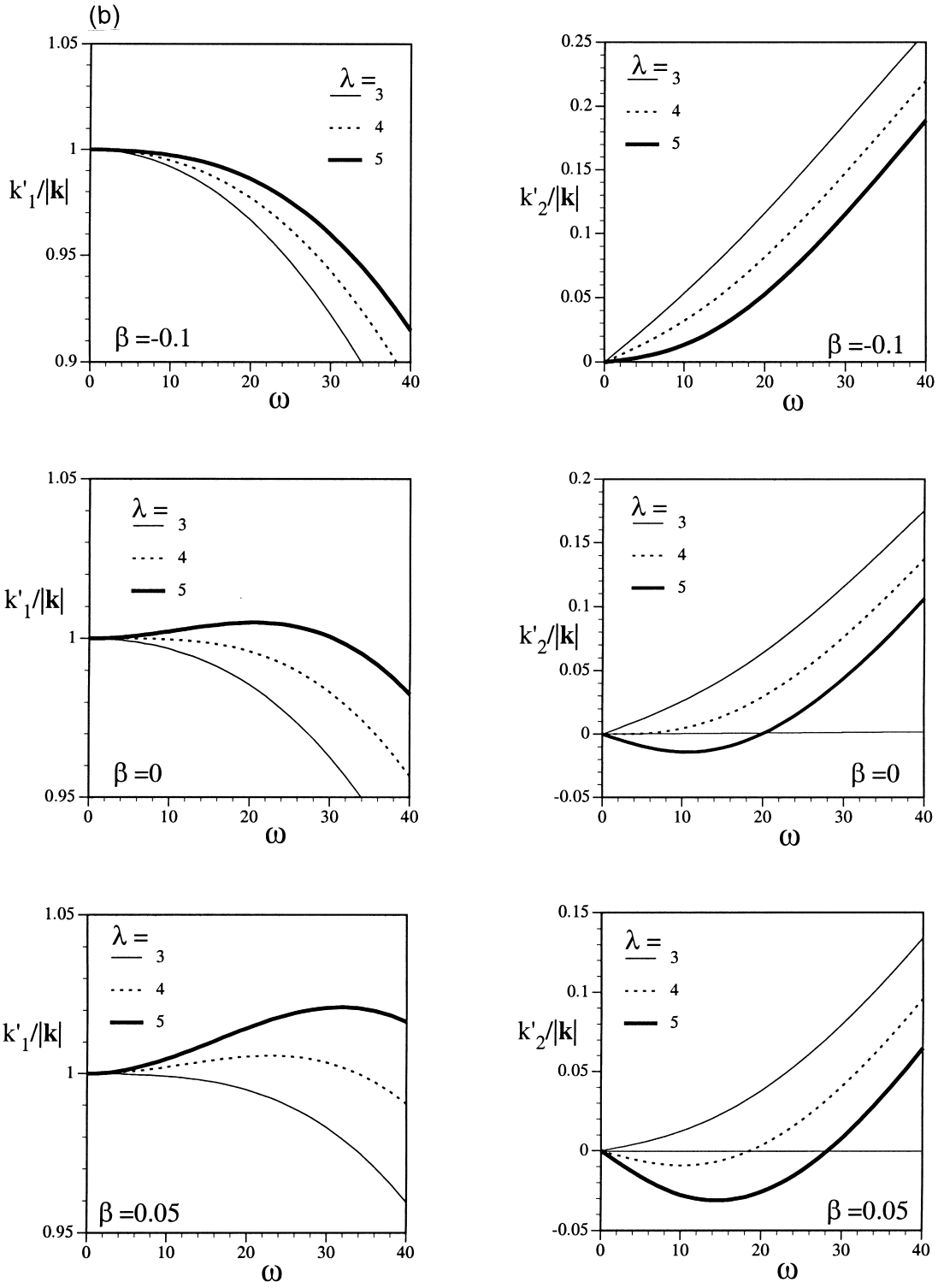

Fig. 3 (*continued*)

errors may arise from material misalignment (or crack orientation) and non-perfect loading locations are sometimes unavoidable in the tests, it is interesting to analyze the kinking behavior of a small material misalignment (or the main crack is aligned close to principal material orientation) under nearly mode-I loading with a small component of mode-II present. To illustrate the effect of these imperfections quantitatively on the kinking behavior, the main crack with orientation $\theta_0 = -5^\circ$ and subjected to mixed-mode loading phase $\psi = \tan^{-1}(k_2/k_1) = 5^\circ$ is investigated. Fig. 3(a) illustrates that stress intensity factors k_1', k_2', and the energy release rate $G(\omega)$ at the kinked crack tip vary with the kink angle ω for three values of the T-stress parameter, $\beta = \sqrt{a}T_1/|\boldsymbol{k}|$, for two materials. One material having $\lambda = 1.1$

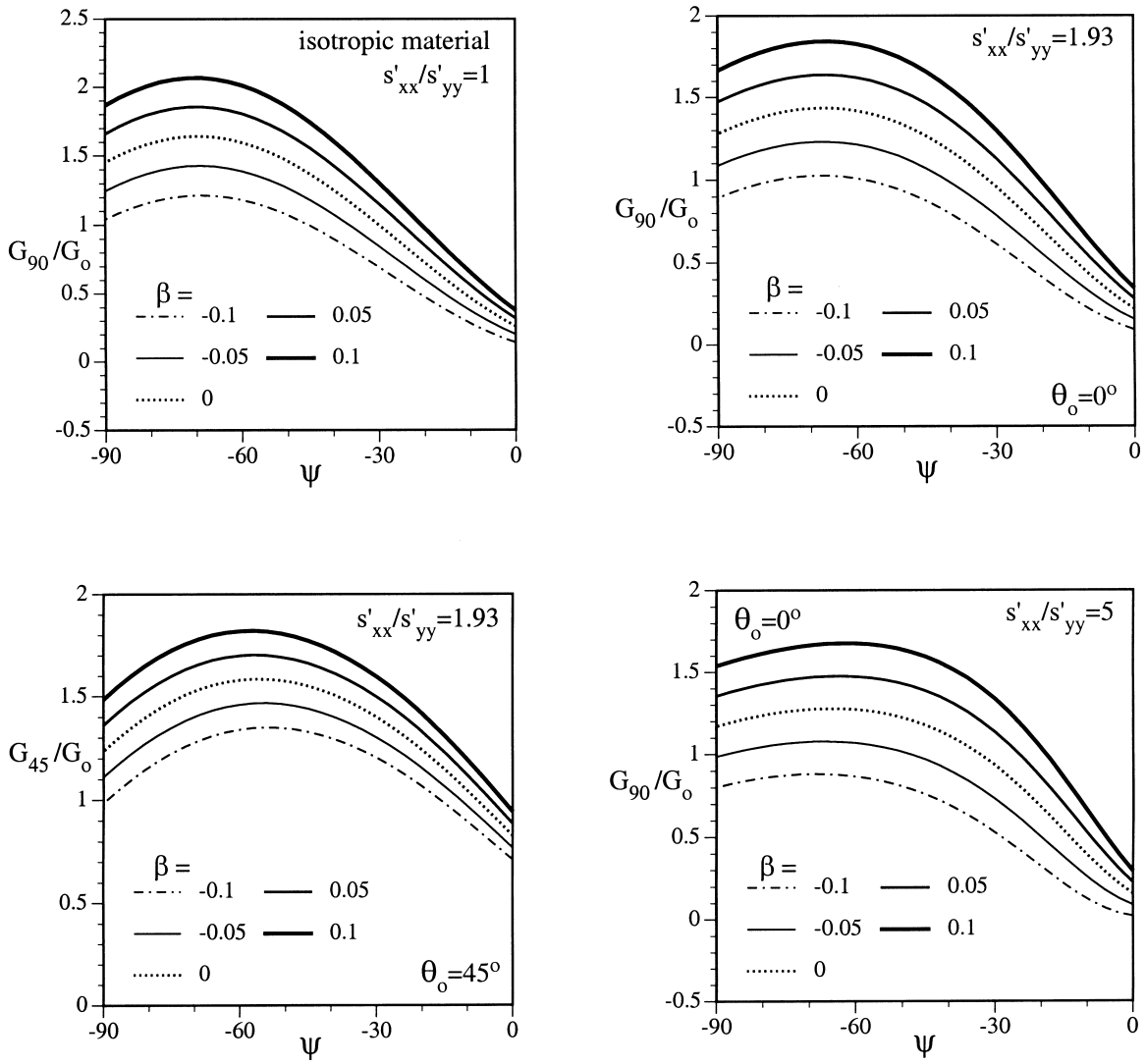

Fig. 4. Energy release rate ratios, G_{90}/G_0 and G_{45}/G_0, as functions of the loading phase ψ for various values of the T-stress parameter β for different degrees of anisotropy.

and $\rho = \sqrt{1.1}$ is considered to be nearly isotropic; the other has a high degree of anisotropy, $\lambda = 5$, $\rho = \sqrt{5}$. In this figure and the sequel, only the first two terms in the expressions of $\boldsymbol{k}'$ and $G(\omega)$, Eqs. (7.12) and (7.16), are included. The effect of higher-order terms with order of a will be discussed later and the figures will be shown in Figs. 14–16. k_1', k_2', and G are normalized by the absolute values, $|\boldsymbol{k}|$ and G_0, respectively. Here $|\boldsymbol{k}|$ and G_0 are the norm of the stress intensity factors and energy release rate at the main crack tip prior to kinking. The T-stress, T_1, has important effect on k_1', k_2', and $G(\omega)$. In the region of $-150^\circ < \omega < 150^\circ$, numerical results indicate that the kinked crack tip is open at $\omega < 140^\circ$ for

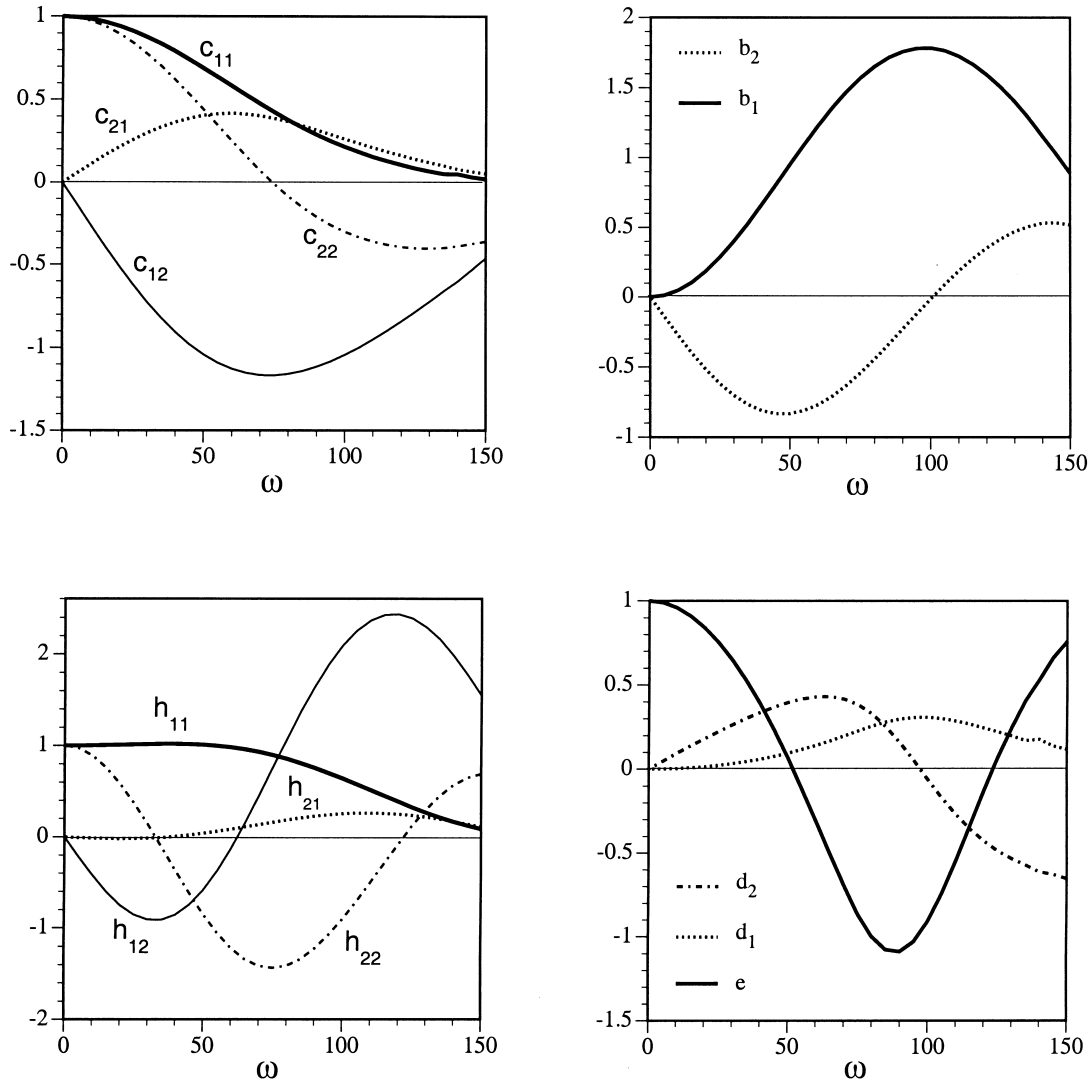

Fig. 5. Variation of coefficients c_{ij}, b_i, h_{ij}, d_i, and e with kink angle ω for $\theta_0 = 0^\circ$. (The main crack is perpendicular to the stiffer material axis of a composite with $\lambda = 1.93$, $\rho = 1.18$).

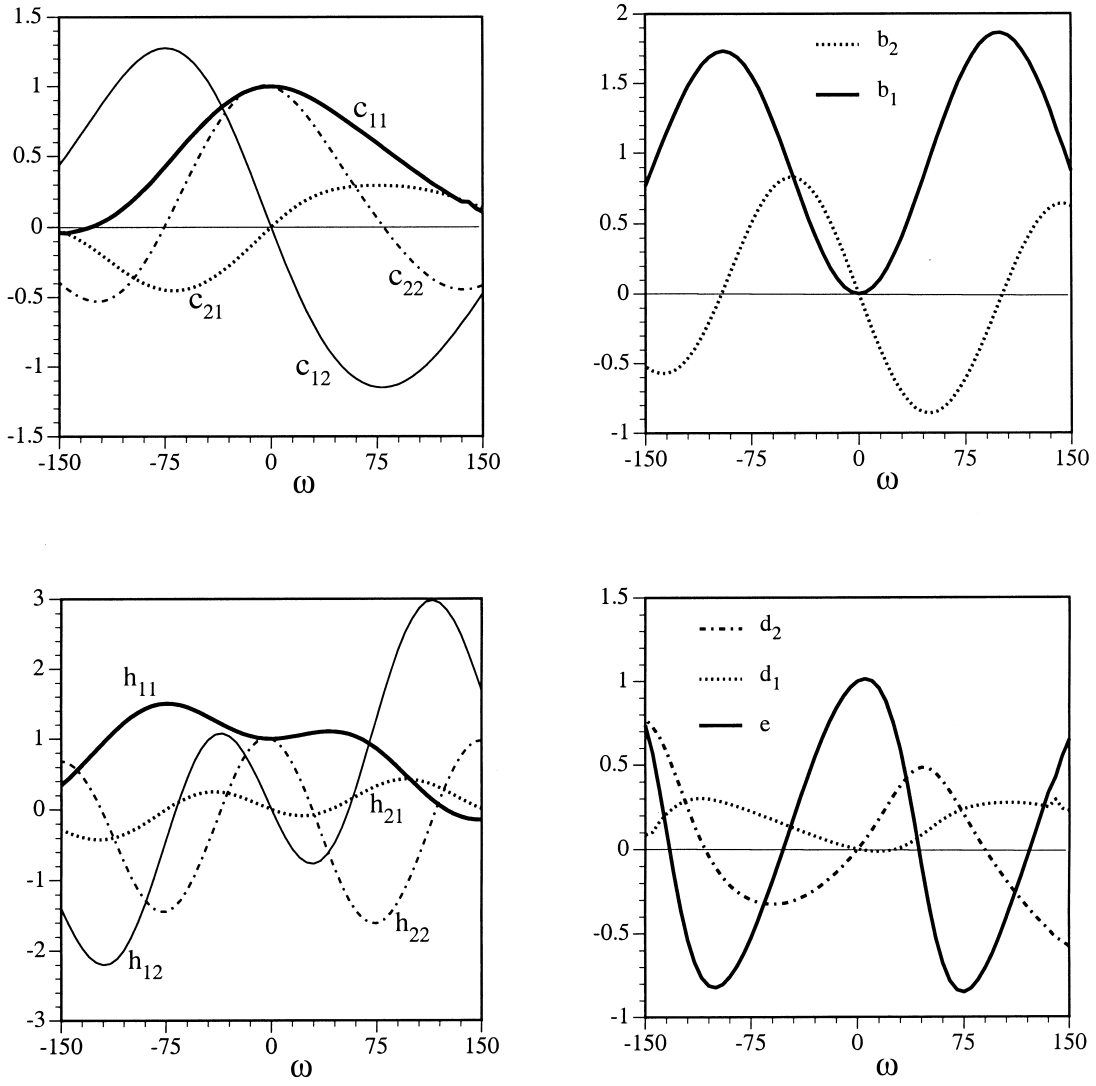

Fig. 6. Variation of coefficients c_{ij}, b_i, h_{ij}, d_i, and e with kink angle ω for $\theta_0 = 45°$. (The main crack makes an angle of 45° with the stiffer material axis of a composite with $\lambda = 1.93$, $\rho = 1.18$).

Table 3
The coefficients as a function of selected ω for $\theta_0 = 0$ in AS4 composite

ω	c_{11}	c_{12}	c_{21}	c_{22}	b_1	b_2	d_1	d_2	e_1	h_{11}	h_{12}	h_{21}	h_{22}
$\pi/4$	0.7391	−0.9790	0.3888	0.5282	0.8094	−0.8315	0.0748	0.3685	0.2347	1.0166	−0.7467	0.0204	−0.6205
$\pi/2$	0.2880	−1.1166	0.3171	−0.2104	1.7582	−0.2279	0.2981	0.1556	−1.0880	0.7563	1.6455	0.2280	−1.2292

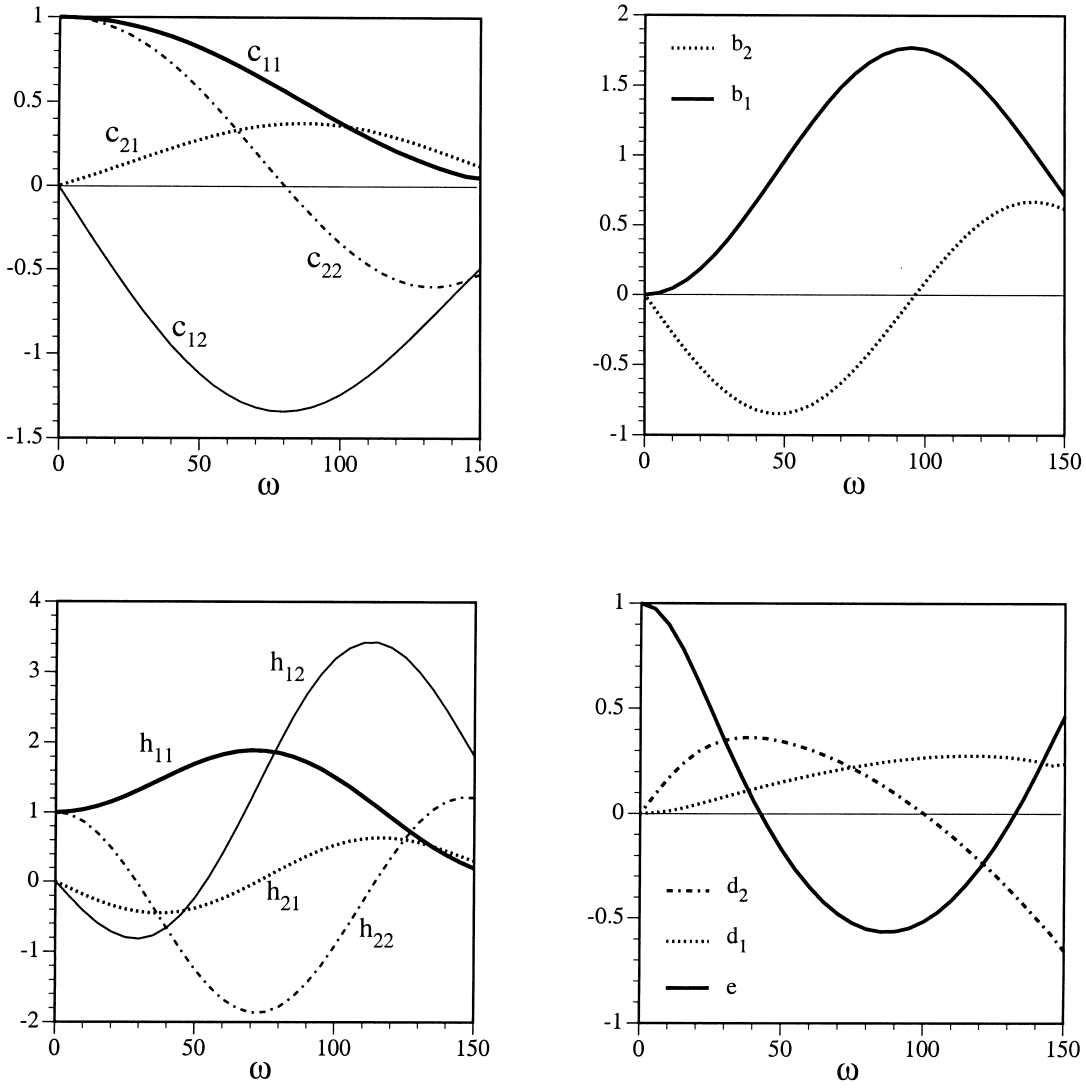

Fig. 7. Variation of coefficients c_{ij}, b_i, h_{ij}, d_i, and e with kink angle ω for $\theta_0 = 90^\circ$. (The main crack is parallel to the stiffer material axis of a composite with $\lambda = 1.93$, $\rho = 1.18$).

Table 4
The coefficients as a function of selected ω for $\theta_0 = 45^\circ$ in AS4 composite

ω	c_{11}	c_{12}	c_{21}	c_{22}	b_1	b_2	d_1	d_2	e_1	h_{11}	h_{12}	h_{21}	h_{22}
$-\pi/2$	0.2628	1.2211	−0.3994	−0.2596	1.7212	0.1548	0.2665	−0.2138	−0.7602	1.4279	−1.3346	−0.1918	−1.2807
$-\pi/4$	0.7606	1.0384	−0.3818	0.6091	0.8089	0.8284	0.1251	−0.3056	0.1887	1.3132	0.9844	0.2447	−0.4665
$\pi/4$	0.8113	−0.9381	0.2657	0.5038	0.8150	−0.8506	0.0816	0.4837	−0.0947	1.1036	−0.4680	0.0247	−0.8419
$\pi/2$	0.4806	−1.1263	0.2890	−0.1346	1.8304	−0.2773	0.2651	−0.0075	−0.7075	0.5912	2.2658	0.4189	−1.3166

Table 5
The coefficients as a function of selected ω for $\theta_0 = \pi/2$ in AS4 composite

ω	c_{11}	c_{12}	c_{21}	c_{22}	b_1	b_2	d_1	d_2	e_1	h_{11}	h_{12}	h_{21}	h_{22}
$\pi/4$	0.8552	−1.0391	0.2509	0.6538	0.8160	−0.8450	0.1348	0.3568	−0.0610	1.6115	−0.4750	−0.4241	−0.9760
$\pi/2$	0.4716	−1.3161	0.3737	−0.1785	1.7582	−0.1641	0.2529	0.0950	−0.5637	1.7204	2.6944	0.3733	−1.4489

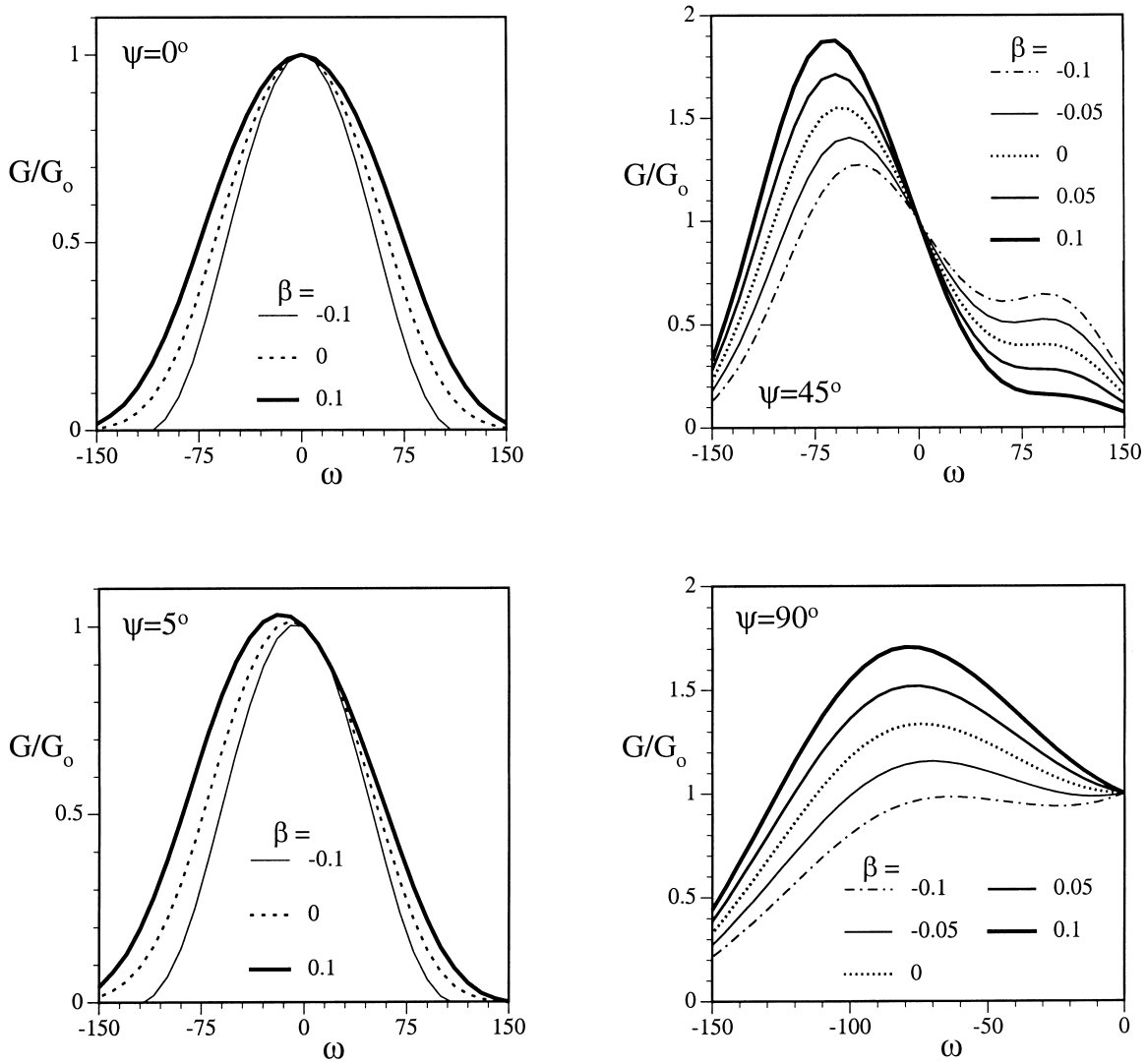

Fig. 8. Energy release rate ratio, G/G_0 as a function of the kink angle ω for various values of loading phase ψ and the T-stress parameter β. The main crack is perpendicular to the stiffer material axis ($\theta_0 = 0°$).

$\rho = 1.1$, and $\omega < 110^\circ$ for $\rho = 5$ (estimated from the condition of opening crack tip, Eq. (3.28)) by selecting $T_1 = 0$. In both cases, the positive T_1 ($\beta > 0$) increases k_1' in the region of interest, and reduces the absolute value $|k_2'|$ in the practically important region, $-90^\circ < \omega < 90^\circ$. In contrast, the negative T-stress ($\beta < 0$) has opposite effect on k_1' and k_2'. As a result, the positive T-stress increases $G(\omega)$ almost in the whole region, especially in the region $\omega < 0$ and shifts $G_{\max}$ to the negative direction of ω. Conversely, the negative T-stress reduces G in $\omega < 0$ and shifts $G_{\max}$ to the positive direction of ω. These effects become more significant with increase of material anisotropy. For the material with stronger anisotropy, $\lambda = 5$, $\rho = \sqrt{5}$, when $|\beta|$ increases 0.05, G_{90}/G_0 can increase by 38%. Note that

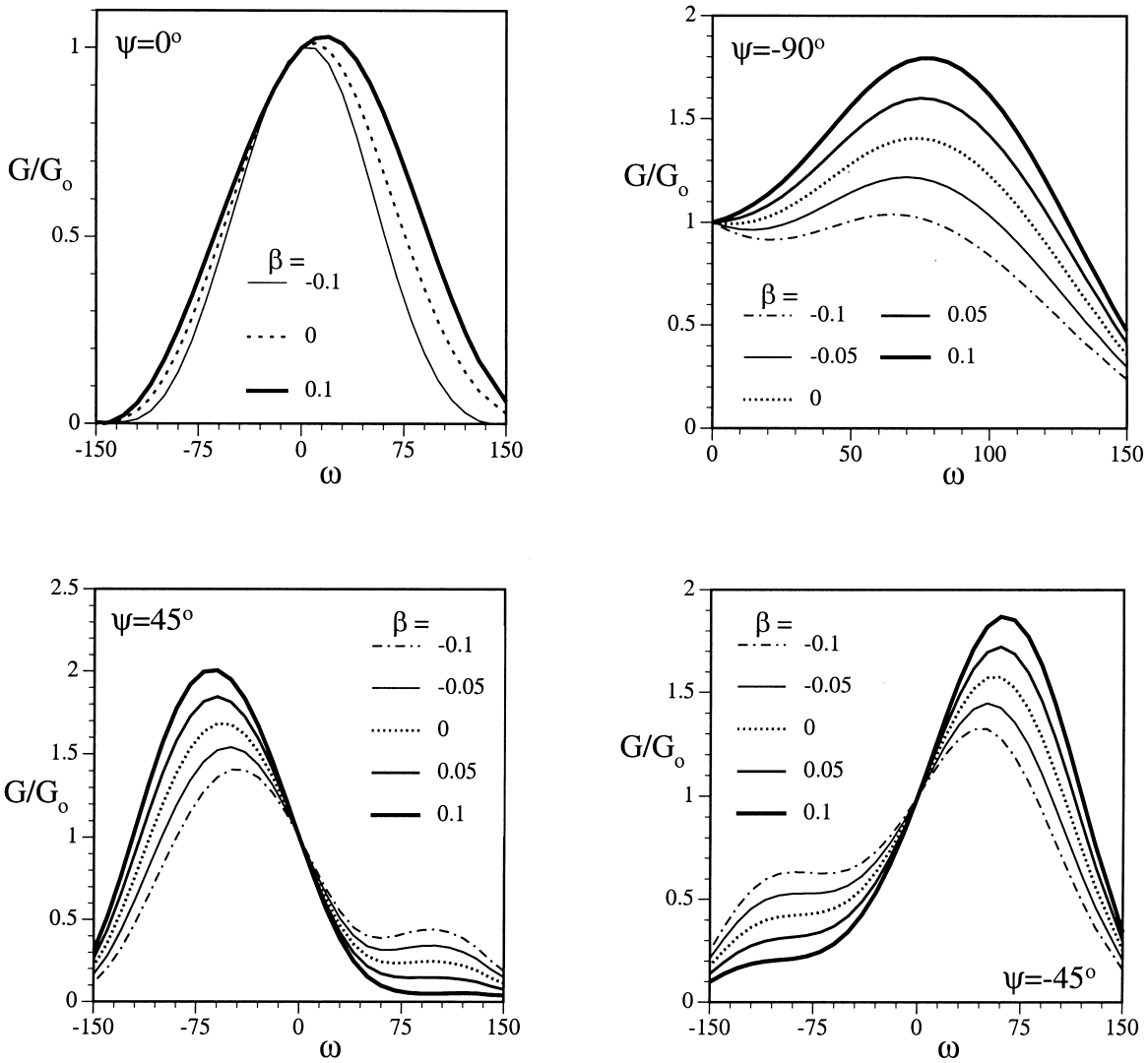

Fig. 9. Energy release rate ratio, G/G_0 as a function of the kink angle ω for various values of loading phase ψ and the T-stress parameter β. The main crack is perpendicular to the stiffer material axis ($\theta_0 = 45^\circ$).

under prefect material alignment and pure mode-I loading for $\theta_0 = 0^\circ$, both the maximum values of $G(\omega)$ and $k_1'(\omega)$ occur at $\omega = 0$ and $k_2'(\omega) = 0$ when $\omega = 0$ exactly. In this example, let ω_c be the kinking angle at which $G(\omega)$, or $k_1'(\omega)$ reaches maximum or $k_2'(\omega) = 0$, then the values of shifted ω_c due to the imperfections are given below:

(i) $\omega_c|_{G=G_{\max}} = -10^\circ$, $\omega_c|_{k_2'=0} = -9.5^\circ$, $\omega_c|_{k_1'=k_{\max}} = -9.5^\circ$, for $\lambda = 1.1$, $\rho = \sqrt{1.1}$, $\beta = 0$

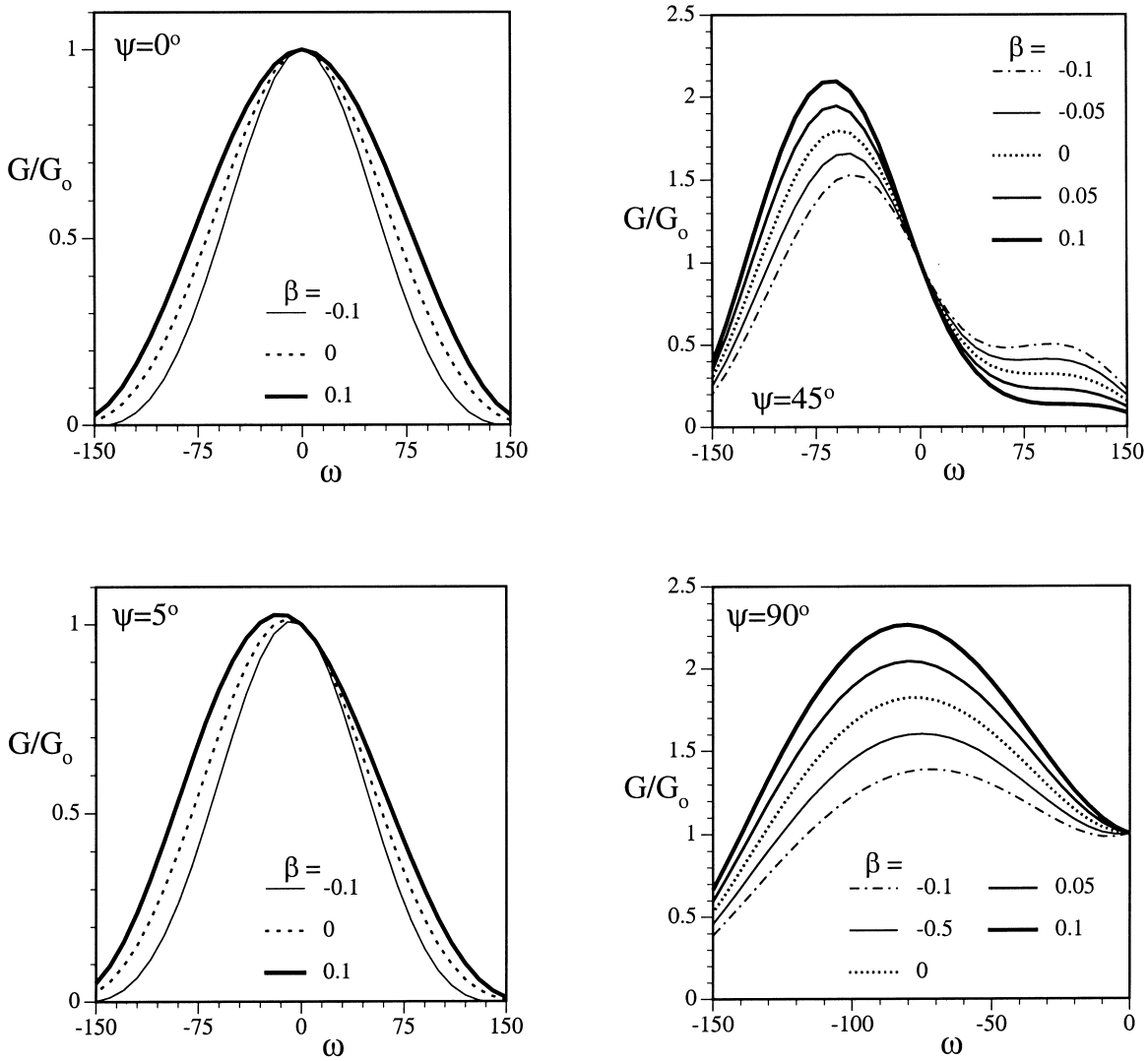

Fig. 10. Energy release rate ratio, G/G_0 as a function of the kink angle ω for various values of loading phase ψ and the T-stress parameter β. The main crack is perpendicular to the stiffer material axis ($\theta_0 = 90^\circ$).

(ii) $\omega_c|_{G=G_{\max}} = -5^\circ$, $\omega_c|_{k_2'=0} = -5^\circ$, $\omega_c|_{k_1'=k_{\max}} = -5^\circ$, for $\lambda = 5$, $\rho = \sqrt{5}$, and $\beta = -0.1$

(iii) $\omega_c|_{G=G_{\max}} = -13^\circ$, $\omega_c|_{k_2'=0} = -6.5^\circ$, $\omega_c|_{k_1'=k_{\max}} = -6.5^\circ$, for $\lambda = 5$, $\rho = \sqrt{5}$, and $\beta = 0$

(iv) $\omega_c|_{G=G_{\max}} = -25^\circ$, $\omega_c|_{k_2'=0} = -8^\circ$, $\omega_c|_{k_1'=k_{\max}} = -9^\circ$, for $\lambda = 5$, $\rho = \sqrt{5}$, and $\beta = 0.1$

For the nearly isotropic materials (case (i)), the kinked angles predicted by the three fracture criteria, maximum G, maximum k_1', and $k_2' = 0$ are essentially identical in this case. However, in the case of high degree of material anisotropy, the kinked angles predicted by the three criteria, in general, can be drastically different for $\beta \geq 0$ and this measurable difference cannot be neglected.

Fig. 3(b) shows the variation of k_1', k_2' with ω under $\beta = -0.1, 0, 0.05$ for three different degrees of material anisotropy, $\lambda = 3, 4, 5$ and corresponding $\rho = \sqrt{\lambda}$. The main crack is parallel to the stiffer

Table 6
Variation of coefficients as a function of kinked angle ω for orthotropic materials $\lambda = 1.93$, $\rho = 1.18$, $\theta_0 = 0^0$

ω	c_{11}	c_{12}	c_{21}	c_{22}	b_1	b_2
0	1	0	0	1	0	0
5	0.9963	−0.1306	0.0557	0.9933	0.0121	−0.1386
10	0.9854	−0.2594	0.1104	0.9735	0.0482	−0.2733
15	0.9675	−0.3848	0.1631	0.9409	0.1071	−0.4003
20	0.9429	−0.5050	0.2128	0.8962	0.1872	−0.5160
25	0.9121	−0.6184	0.2587	0.8402	0.2862	−0.6173
30	0.8755	−0.7237	0.2999	0.7739	0.4013	−0.7014
35	0.8340	−0.8196	0.3357	0.6988	0.5393	−0.7660
40	0.7882	−0.9049	0.3655	0.6163	0.6666	−0.8097
45	0.7391	−0.9790	0.3888	0.5282	0.8094	−0.8315
50	0.6874	−1.0410	0.4052	0.4362	0.9538	−0.8312
55	0.6342	−1.0907	0.4146	0.3424	1.0959	−0.8095
60	0.5803	−1.1280	0.4171	0.2488	1.2320	−0.7675
65	0.5267	−1.1530	0.4129	0.1573	1.3586	−0.7071
70	0.4742	−1.1661	0.4025	0.0699	1.4726	−0.6308
75	0.4235	−1.1682	0.3868	−0.0118	1.5714	−0.5416
80	0.3753	−1.1599	0.3665	−0.0862	1.6529	−0.4425
85	0.3300	−1.1424	0.3429	−0.1526	1.7155	−0.3369
90	0.2880	−1.1166	0.3171	−0.2104	1.7582	−0.2279
95	0.2494	−1.0837	0.2901	−0.2596	1.7804	−0.1185
100	0.2143	−1.0446	0.2628	−0.3005	1.7819	−0.0111
105	0.1825	−1.0002	0.2360	−0.3338	1.7632	0.0918
110	0.1540	−0.9513	0.2101	−0.3599	1.7248	0.1882
115	0.1285	−0.8986	0.1854	−0.3795	1.6678	0.2762
120	0.1059	−0.8426	0.1621	−0.3928	1.5933	0.3538
125	0.0860	−0.7840	0.1402	−0.4003	1.5032	0.4195
130	0.0684	−0.7232	0.1198	−0.4020	1.3993	0.4716
135	0.0523	−0.6603	0.1012	−0.3982	1.2842	0.5086
140	0.0494	−0.6005	0.0797	−0.3870	1.1529	0.5323
145	0.0321	−0.5328	0.0664	−0.3736	1.0248	0.5351
150	0.0208	−0.4613	0.0538	−0.3597	0.8908	0.5202

material direction, $\theta_0 = 90^\circ$, and subjected to mode-I loading. It is shown that the variation of k_1', k_2' for different T-stress levels is quite different. ω_c is given by $G(\omega_c) = G_{\max}$ is $\omega_c = 0$ for all cases (not shown in the figure). But ω_c determined by $k_1'(\omega) = (k_1')_{\max}$ and $k_2'(\omega) = 0$ are listed below:

$$\omega_c|_{k_2'=0} = 0, \quad \omega_c|_{k_1'=k_{\max}} = 0, \quad \text{for } \lambda = 3,\ \beta = -0.1, 0, 0.05;$$

$$\omega_c|_{k_2'=0} = 0, \quad \omega_c|_{k_1'=k_{\max}} = 0, \quad \text{for } \lambda = 4 \text{ and } 5,\ \beta = -0.1$$

However,

$$\omega_c|_{k_2'=0} = 0^\circ, \pm 20^\circ, \quad \omega_c|_{k_1'=k_{\max}} = \pm 20.5^\circ, \quad \text{for } \lambda = 5,\ \beta = 0$$

Table 7
Variation of coefficients as a function of kinked angle ω for orthotropic materials $\lambda = 1.93$, $\rho = 1.18$, $\theta_0 = 0^\circ$

ω	h_{11}	h_{12}	h_{21}	h_{22}	d_1	d_2	e
0	1	0	0	1	0	0	1
5	1.0008	−0.2162	−0.0068	0.9725	0.0009	0.0463	0.9899
10	1.0029	−0.4204	−0.0128	0.8913	0.0035	0.0921	0.9596
15	1.0062	−0.6012	−0.0172	0.7602	0.0079	0.1371	0.9097
20	1.0102	−0.7484	−0.0193	0.5851	0.0141	0.1809	0.8408
25	1.0143	−0.8531	−0.0184	0.3741	0.0221	0.2230	0.7536
30	1.0178	−0.9087	−0.0142	0.1370	0.0320	0.2633	0.6488
35	1.0199	−0.9104	−0.0064	−0.1154	0.0440	0.3013	0.5271
40	1.0198	−0.8562	0.0052	−0.3718	0.0581	0.3367	0.3889
45	1.0166	−0.7467	0.0204	−0.6205	0.0748	0.3685	0.2347
50	1.0095	−0.5847	0.0390	−0.8506	0.0940	0.3958	0.0654
55	0.9978	−0.3755	0.0606	−1.0521	0.1161	0.4168	−0.1173
60	0.9809	−0.1264	0.0844	−1.2167	0.1410	0.4293	−0.3099
65	0.9582	0.1535	0.1098	−1.3378	0.1685	0.4300	−0.5061
70	0.9296	0.4541	0.1358	−1.4114	0.1978	0.4153	−0.6961
75	0.8949	0.7645	0.1616	−1.4357	0.2277	0.3818	−0.8658
80	0.8542	1.0736	0.1861	−1.4113	0.2560	0.3270	−0.9982
85	0.8078	1.3706	0.2085	−1.3409	0.2803	0.2505	−1.0763
90	0.7563	1.6455	0.2280	−1.2292	0.2981	0.1556	−1.0880
95	0.7003	1.8893	0.2437	−1.0823	0.3075	0.0485	−1.0298
100	0.6407	2.0945	0.2550	−0.9069	0.3080	−0.0628	−0.9090
105	0.5784	2.2549	0.2616	−0.7109	0.3002	−0.1706	−0.7408
110	0.5147	2.3661	0.2629	−0.5021	0.2858	−0.2690	−0.5438
115	0.4507	2.4256	0.2590	−0.2889	0.2667	−0.3548	−0.3354
120	0.3876	2.4325	0.2498	−0.0794	0.2448	−0.4270	−0.1290
125	0.3266	2.3878	0.2356	0.1181	0.2214	−0.4864	−0.0665
130	0.2689	2.2945	0.2170	0.2961	0.1972	−0.5341	−0.2461
135	0.2154	2.1572	0.1945	0.4475	0.1709	−0.5712	0.4084
140	0.1670	1.9768	0.1693	0.5685	0.1767	−0.6128	0.5315
145	0.1247	1.7723	0.1421	0.6497	0.1374	−0.6290	0.6622
150	0.0887	1.5436	0.1141	0.6901	0.1178	−0.6541	0.7586

Table 8
Variation of coefficients as a function of kinked angle ω for orthotropic materials $\lambda = 1.93$, $\rho = 1.18$, $\theta_0 = 45^\circ$

ω	c_{11}	c_{12}	c_{21}	c_{22}	b_1	b_2
−150	−0.0374	0.4387	−0.0192	−0.3943	0.7686	−0.5222
−145	−0.0415	0.5052	−0.0416	−0.4349	0.8993	−0.5530
−140	−0.0311	0.5770	−0.0645	−0.4697	1.0243	−0.5702
−135	−0.0212	0.6494	−0.0928	−0.4983	1.1481	−0.5700
−130	−0.0076	0.7229	−0.1248	−0.5184	1.2667	−0.5521
−125	0.0101	0.7968	−0.1598	−0.5285	1.3775	−0.5159
−120	0.0323	0.8700	−0.1967	−0.5273	1.4775	−0.4613
−115	0.0592	0.9415	−0.2346	−0.5137	1.5643	−0.3892
−110	0.0910	1.0098	−0.2723	−0.4873	1.6352	−0.3013
−105	0.1275	1.0734	−0.3086	−0.4480	1.6879	−0.1997
−100	0.1685	1.1307	−0.3425	−0.3964	1.7206	−0.0876
−95	0.2138	1.1804	−0.3731	−0.3332	1.7320	0.0319
−90	0.2628	1.2211	−0.3994	−0.2596	1.7212	0.1548
−85	0.3150	1.2514	−0.4210	−0.1769	1.6882	0.2774
−80	0.3697	1.2703	−0.4371	−0.0865	1.6333	0.3957
−75	0.4263	1.2770	−0.4474	0.0097	1.5578	0.5060
−70	0.4840	1.2707	−0.4517	0.1100	1.4635	0.6046
−65	0.5419	1.2510	−0.4498	0.2127	1.3527	0.6885
−60	0.5994	1.2178	−0.4417	0.3157	1.2284	0.7547
−55	0.6555	1.1711	−0.4275	0.4174	1.0938	0.8011
−50	0.7095	1.1111	−0.4074	0.5157	0.9527	0.8260
−45	0.7606	1.0384	−0.3818	0.6091	0.8089	0.8284
−40	0.8082	0.9538	−0.3510	0.6957	0.6664	0.8080
−35	0.8515	0.8583	−0.3156	0.7740	0.5293	0.7653
−30	0.8900	0.7529	−0.2763	0.8427	0.4013	0.7011
−25	0.9232	0.6392	−0.2336	0.9005	0.2862	0.6173
−20	0.9508	0.5185	−0.1885	0.9464	0.1872	0.5161
−15	0.9724	0.3925	−0.1417	0.9797	0.1071	0.4004
−10	0.9878	0.2629	−0.0941	0.9998	0.0482	0.2733
−5	0.9969	0.1315	−0.0465	1.0065	0.0121	0.1386
0	1	0	0	1	0	0
5	0.9970	−0.1298	0.0447	0.9806	0.0121	−0.1386
10	0.9884	−0.2561	0.0867	0.9490	0.0482	−0.2734
15	0.9745	−0.3775	0.1253	0.9063	0.1071	−0.4007
20	0.9558	−0.4926	0.1599	0.8539	0.1873	−0.5170
25	0.9328	−0.6001	0.1900	0.7933	0.2865	−0.6196
30	0.9063	−0.6990	0.2155	0.7262	0.4022	−0.7058
35	0.8768	−0.7886	0.2364	0.6545	0.5311	−0.7738
40	0.8450	−0.8684	0.2530	0.5799	0.6699	−0.8223
45	0.8113	−0.9381	0.2657	0.5038	0.8150	−0.8506
50	0.7764	−0.9977	0.2753	0.4274	0.9629	−0.8582
55	0.7405	−1.0472	0.2824	0.3516	1.1097	−0.8454
60	0.7040	−1.0867	0.2874	0.2767	1.2519	−0.8126
65	0.6671	−1.1164	0.2909	0.2031	1.3860	−0.7608
70	0.6299	−1.1366	0.2930	0.1311	1.5088	−0.6913
75	0.5925	−1.1474	0.2939	0.0609	1.6170	−0.6057
80	0.5551	−1.1491	0.2936	−0.0071	1.7082	−0.5064
85	0.5178	−1.1419	0.2920	−0.0725	1.7799	−0.3960
90	0.4806	−1.1263	0.2890	−0.1346	1.8304	−0.2273
95	0.4438	−1.1025	0.2845	−0.1930	1.8583	−0.1537
100	0.4074	−1.0709	0.2784	−0.2468	1.8631	−0.0286

Table 8 (*continued*)

ω	c_{11}	c_{12}	c_{21}	c_{22}	b_1	b_2
105	0.3717	−1.0322	0.2706	−0.2955	1.8445	0.0944
110	0.3367	−0.9869	0.2612	−0.3383	1.8031	0.2120
115	0.3027	−0.9356	0.2501	−0.3747	1.7398	0.3207
120	0.2698	−0.8790	0.2373	−0.4041	1.6563	0.4174
125	0.2380	−0.8179	0.2231	−0.4260	1.5547	0.4993
130	0.2075	−0.7531	0.2074	−0.4401	1.4376	0.5641
135	0.1776	−0.6850	0.1906	−0.4459	1.3082	0.6096
140	0.1757	−0.6212	0.1683	−0.4424	1.1574	0.6367
145	0.1308	−0.5449	0.1528	−0.4324	1.0205	0.6390
150	0.1055	−0.4706	0.1345	−0.4150	0.8729	0.6205

Table 9
Variation of coefficients as a function of kinked angle ω for orthotropic materials $\lambda = 1.93$, $\rho = 1.18$, $\theta_0 = 45^\circ$

ω	h_{11}	h_{12}	h_{21}	h_{22}	d_1	d_2	e
−150	0.3489	−1.3924	−0.2828	0.6851	0.0857	0.7781	0.7372
−145	0.4362	−1.6068	−0.3246	0.6554	0.1026	0.7280	0.5720
−140	0.5298	−1.7965	−0.3611	0.5858	0.1653	0.6670	0.3467
−135	0.6293	−1.9588	−0.3904	0.4754	0.2092	0.5783	0.1064
−130	0.7326	−2.0848	−0.4108	0.3275	0.2455	0.4723	−0.1340
−125	0.8376	−2.1679	−0.4211	0.1468	0.2730	0.3578	−0.3537
−120	0.9421	−2.2026	−0.4204	−0.0596	0.2909	0.2435	−0.5364
−115	1.0437	−2.1853	−0.4080	−0.2830	0.3001	0.1363	−0.6738
−110	1.1399	−2.1141	−0.3841	−0.5130	0.3019	0.0406	−0.7645
−105	1.2285	−1.9895	−0.3492	−0.7387	0.2979	−0.0418	−0.8124
−100	1.3072	−1.8143	−0.3044	−0.9488	0.2899	−0.1110	−0.8234
−95	1.3742	−1.5936	−0.2513	−1.1326	0.2791	−0.1678	−0.8040
−90	1.4279	−1.3346	−0.1918	−1.2807	0.2665	−0.2138	−0.7602
−85	1.4673	−1.0463	−0.1182	−1.3851	0.2527	−0.2503	−0.6966
−80	1.4918	−0.7393	−0.0630	−1.4401	0.2381	−0.2788	−0.6170
−75	1.5016	−0.4250	0.0013	−1.4421	0.2229	−0.3001	−0.5242
−70	1.4970	−0.1154	0.0622	−1.3904	0.2073	−0.3149	−0.4205
−65	1.4793	0.1778	0.1173	−1.2866	0.1913	−0.3238	−0.3081
−60	1.4500	0.4435	0.1645	−1.1348	0.1750	−0.3272	−0.1889
−55	1.4109	0.6716	0.2023	−0.9416	0.1585	−0.3251	−0.0649
−50	1.3645	0.8540	0.2292	−0.7155	0.1418	−0.3179	0.0617
−45	1.3132	0.9844	0.2447	−0.4665	0.1251	−0.3056	0.1887
−40	1.2596	1.0590	0.2485	−0.2059	0.1085	−0.2886	0.3139
−35	1.2063	1.0764	0.2409	0.0545	0.0922	−0.2670	0.4349
−30	1.1557	1.0379	0.2230	0.3028	0.0764	−0.2411	0.5496
−25	1.1099	0.9475	0.1960	0.5276	0.0611	−0.2111	0.6561
−20	1.0707	0.8113	0.1619	0.7187	0.0466	−0.1770	0.7526
−15	0.0396	0.6378	0.1228	0.8671	0.0331	−0.1390	0.8373
−10	0.0174	0.4370	0.0811	0.9661	0.0207	−0.0970	0.9083
−5	0.0042	0.2204	0.0393	1.0111	0.0096	−0.0507	0.9634

(continued on next page)

Table 9 (*continued*)

ω	h_{11}	h_{12}	h_{21}	h_{22}	d_1	d_2	e
0	1	0	0	1	0	0	1
5	1.0039	−0.2119	−0.0344	0.9333	−0.0076	0.0554	1.0144
10	1.0145	−0.4033	−0.0619	0.8139	−0.0127	0.1154	1.0022
15	1.0302	−0.5633	−0.0806	0.6471	−0.0146	0.1795	0.9580
20	1.0488	−0.6822	−0.0893	0.4405	−0.0125	0.2463	0.8766
25	1.0680	−0.7523	−0.0872	0.2030	−0.0053	0.3133	0.7533
30	1.0855	−0.7680	−0.0741	−0.0549	0.0076	0.3762	0.5868
35	1.0987	−0.7260	−0.0504	−0.3225	0.0269	0.4294	0.3813
40	1.1054	−0.6254	−0.0170	−0.5884	0.0520	0.4670	0.1481
45	1.1036	−0.4680	0.0247	−0.8419	0.0816	0.4837	−0.0947
50	1.0916	−0.2577	0.0730	−1.0727	0.1136	0.4771	−0.3255
55	0.0681	−0.0009	0.1255	−1.2715	0.1453	0.4480	−0.5247
60	0.0326	0.2945	0.1801	−1.4304	0.1745	0.4003	−0.6789
65	0.9847	0.6186	0.2342	−1.5429	0.1998	0.3395	−0.7827
70	0.9249	0.9604	0.2855	−1.6042	0.2205	0.2711	−0.8380
75	0.8540	1.3082	0.3315	−1.6116	0.2369	0.1997	−0.8507
80	0.7735	1.6496	0.3702	−1.5645	0.2493	0.1284	−0.8285
85	0.6852	1.9726	0.3998	−1.4649	0.2585	0.0590	−0.7786
90	0.5912	2.2658	0.4189	−1.3166	0.2651	−0.0075	−0.7075
95	0.4941	2.5187	0.4268	−1.1260	0.2695	−0.0709	−0.6199
100	0.3964	2.7226	0.4230	−0.9010	0.2723	−0.1312	−0.5197
105	0.3008	2.8705	0.4077	−0.6513	0.2736	−0.1888	−0.4097
110	0.2097	2.9577	0.3817	−0.3876	0.2734	−0.2436	−0.2923
115	0.1257	2.9820	0.3463	−0.1213	0.2719	−0.2959	−0.1696
120	0.0506	2.9435	0.3030	0.1364	0.2688	−0.3455	−0.0435
125	−0.0139	2.8448	0.2540	0.3744	0.2641	−0.3923	0.0837
130	−0.0664	2.6908	0.2014	0.5827	0.2573	−0.4361	0.2101
135	−0.1064	2.4888	0.1479	0.7527	0.2466	−0.4760	0.3340
140	−0.1325	1.2377	0.0956	0.8790	0.2917	−0.5265	0.4261
145	−0.1480	1.9729	0.0477	0.9527	0.2380	−0.5497	0.5533
150	−0.1512	1.6830	0.0059	0.9746	0.2248	−0.5812	0.6506

$$\omega_c|_{k_2'=0} = 0^\circ, \pm 19^\circ, \quad \omega_c|_{k_1'=k_{\max}} = \pm 23^\circ, \quad \text{for } \lambda = 4,\ \beta = 0.05$$

$$\omega_c|_{k_2'=0} = 0^\circ, \pm 28^\circ, \quad \omega_c|_{k_1'=k_{\max}} = \pm 32^\circ, \quad \text{for } \lambda = 5,\ \beta = 0.05$$

In the above three cases, $k_2' = 0$ provides three solutions for ω_c and $k_1'|_{\omega=0}$ becomes local minimum shown in the figure. If the g-term is included in the calculation, a similar characteristic still remains. The value of $k_1'|_{\omega=0}$ being the local minimum for strong material anisotropy was observed by Gao and Chiu (1992) based on a perturbation solution and $\beta = 0$. Because the fracture resistance at $\omega = 0$ (along the stiffer direction) is, in general, lower compared with other directions, based on the energy release rate criterion, the crack extension will usually take place at $G(\omega)|_{\omega=0} = G_c$. Since $\boldsymbol{b} = 0$ at $\omega = 0$, the stability condition of the kinked crack tip is controlled by the g-term according to Eq. (7.25).

Table 10
Variation of coefficients as a function of kinked angle ω for orthotropic materials $\lambda = 1.93$, $\rho = 1.18$, $\theta_0 = 90^\circ$

ω	c_{11}	c_{12}	c_{21}	c_{22}	b_1	b_2
0	1	0	0	1	0	0
5	0.9982	−0.1307	0.0267	0.9960	0.0121	−0.1387
10	0.9930	−0.2603	0.0537	0.9839	0.0482	−0.2737
15	0.9842	−0.3877	0.0812	0.9634	0.1072	−0.4014
20	0.9718	−0.5116	0.1094	0.9342	0.1875	−0.5185
25	0.9557	−0.6310	0.1380	0.8960	0.2871	−0.6216
30	0.9360	−0.7446	0.1669	0.8487	0.4031	−0.7080
35	0.9126	−0.8513	0.1956	0.7922	0.5323	−0.7752
40	0.8856	−0.9498	0.2238	0.7271	0.6712	−0.8213
45	0.8552	−1.0391	0.2509	0.6538	0.8160	−0.8450
50	0.8214	−1.1182	0.2764	0.5733	0.9626	−0.8457
55	0.7846	−1.1863	0.2997	0.4865	1.1070	−0.8234
60	0.7450	−1.2426	0.3205	0.3948	1.2452	−0.7790
65	0.7030	−1.2866	0.3384	0.2994	1.3735	−0.7137
70	0.6590	−1.3180	0.3530	0.2019	1.4883	−0.6297
75	0.6134	−1.3365	0.3640	0.1038	1.5864	−0.5295
80	0.5666	−1.3422	0.3712	0.0066	1.6654	−0.4162
85	0.5192	−1.3352	0.3745	−0.0880	1.7231	−0.2931
90	0.4716	−1.3161	0.3737	−0.1785	1.7582	−0.1641
95	0.4243	−1.2854	0.3690	−0.2635	1.7697	−0.0329
100	0.3778	−1.2438	0.3603	−0.3415	1.7577	0.0965
105	0.3326	−1.1924	0.3478	−0.4112	1.7226	0.2203
110	0.2892	−1.1321	0.3317	−0.4715	1.6655	0.3348
115	0.2478	−1.0641	0.3122	−0.5213	1.5883	0.4368
120	0.2090	−0.9899	0.2897	−0.5596	1.4933	0.5231
125	0.1731	−0.9106	0.2645	−0.5859	1.3831	0.5914
130	0.1403	−0.8278	0.2372	−0.5995	1.2608	0.6397
135	0.1108	−0.7429	0.2082	−0.6002	1.1299	0.6668
140	0.0847	−0.6572	0.1783	−0.5879	0.9937	0.6721
145	0.0606	−0.5716	0.1484	−0.5627	0.8562	0.6556
150	0.0495	−0.4905	0.1179	−0.5252	0.7169	0.6186

$$\tilde{\alpha}_1 < 0 \quad \text{at } \omega = 0$$

that is, if $g_1 < 0$, the kinked crack is stable and vice versa.

For fiber reinforced composites, a dominant crack tends to deflect into the stiffer material direction. It is assumed that the stiffer material orientation coincides with principal material Y-axis. If the crack is perpendicular to the stiffer direction, $\theta_0 = 0^\circ$, the kinking along the stiffer direction can be described by $G_{90} = G(\omega)|_{\omega=90}$ or $G_{-90} = G(\omega)|_{\omega=-90}$. Three figures presented in Fig. 4 provide G_{90}/G_0 as a function of loading phase ψ for a variety of T-stress levels described by β for two anisotropic materials. For comparison purposes, the case of isotropic materials is also shown. The two anisotropic materials have material constants: $\lambda = 1.93$, $\rho = 1.18$; and $\lambda = 5$, $\rho = \sqrt{5}$. Clearly, the positive β increases G_{90} and vice versa regardless of the loading phase. G_{90} reaches maximum around the loading phase angle $\psi = -66^\circ$ for the two anisotropic materials, $\psi = -69^\circ$ for isotropic materials. When the value of β increases 0.1,

Table 11
Variation of coefficients as a function of kinked angle ω for orthotropic materials $\lambda = 1.93$, $\rho = 1.18$, $\theta_0 = 90^\circ$

ω	h_{11}	h_{12}	h_{21}	h_{22}	d_1	d_2	e
0	1	0	0	1	0	0	1
5	1.0103	−0.2157	−0.0939	0.9664	0.0032	0.0882	0.9737
10	1.0407	−0.4167	−0.1838	0.8669	0.0124	0.1692	0.8986
15	1.0899	−0.5891	−0.2658	0.7063	0.0263	0.2376	0.7852
20	1.1557	−0.7202	−0.3362	0.4919	0.0432	0.2905	0.6470
25	1.2351	−0.7993	−0.3919	0.2337	0.0617	0.3277	0.4968
30	1.3247	−0.8182	−0.4301	−0.0562	0.0807	0.3508	0.3451
35	1.4203	−0.7714	−0.4488	−0.3642	0.0994	0.3618	0.1991
40	1.5174	−0.6567	−0.4469	−0.6757	0.1175	0.3632	0.0630
45	1.6115	−0.4750	−0.4241	−0.9760	0.1348	0.3568	−0.0610
50	1.6980	−0.2306	−0.3809	−1.2508	0.1512	0.3443	−0.1720
55	1.7725	0.0695	−0.3188	−1.4871	0.1669	0.3266	−0.2695
60	1.8311	0.4154	−0.2403	−1.6735	0.1818	0.3046	−0.3536
65	1.8705	0.7950	−0.1483	−1.8011	0.1960	0.2785	−0.4241
70	1.8882	1.1945	−0.0466	−1.8637	0.2094	0.2488	−0.4808
75	1.8823	1.5991	0.0608	−1.8583	0.2219	0.2154	−0.5234
80	1.8521	1.9937	0.1695	−1.7847	0.2334	0.1786	−0.5516
85	1.7977	2.3634	0.2751	−1.6462	0.2438	0.1384	−0.5651
90	1.7204	2.6944	0.3733	−1.4489	0.2529	0.0950	−0.5637
95	1.6220	2.9744	0.4602	−1.2016	0.2606	0.0486	−0.5475
100	1.5055	3.1932	0.5326	−0.9156	0.2668	−0.0007	−0.5168
105	1.3743	3.3435	0.5878	−0.6035	0.2715	−0.0528	−0.4718
110	1.2323	3.4205	0.6239	−0.2795	0.2745	−0.1077	−0.4133
115	1.0840	3.4228	0.6401	0.0421	0.2759	−0.1653	−0.3417
120	0.9336	3.3518	0.6362	0.3469	0.2754	−0.2257	−0.2577
125	0.7855	3.2120	0.6133	0.6218	0.2730	−0.2893	−0.1617
130	0.6439	3.0108	0.5733	0.8547	0.2683	−0.3561	−0.0542
135	0.5121	2.7576	0.5188	1.0360	0.2609	−0.4262	0.0643
140	0.3933	2.4638	0.4531	1.1585	0.2496	−0.4993	0.1930
145	0.2896	2.1425	0.3801	1.2178	0.2293	−0.5734	0.3313
150	0.2022	1.8029	0.3040	1.2132	0.2366	−0.6576	0.4633

the ratio G_{90}/G_0 increases about 25% for $\lambda = 1.93$, $\rho = 1.18$, 30% for $\lambda = 5$, $\rho = \sqrt{5}$, in the region of $-90^\circ < \psi < -33^\circ$. The results show that, under mixed-mode loading in the region of $-90^\circ < \psi < -33^\circ$, $G_{90}/G_0 > 1$ if $\beta \geq 0$. This suggests that if the fracture resistance along the stiffer material direction is the lowest, kink is likely to occur along this direction. The variation of G_{-90} with respect to ψ can be obtained by simply replacing G_{90} by G_{-90}, $-G_{-90}$, $-\psi$ by ψ. Similar conclusions can be made for kinking along $\omega = -90^\circ$ when $\psi < 0$. When crack orientation $\theta_0 = 45^\circ$, the kinking along the stiffer direction is controlled by G_{45}. The variation of G_{45} with ψ for different β is also shown in Fig. 4. The material constants are $\lambda = 1.93$, $\rho = 1.18$. $G_{45}/G_0 > 1$ when $-90^\circ < \psi < -20^\circ$ and $\beta > -0.1$. In this case, kink is likely to take place along this stiffer direction. Fig. 4 indicates that the stability of the kinked crack along $\omega = 90^\circ$ or 45° is controlled by the T-stress, that is, the negative T-stress can create stable kinked crack along these directions and vice versa. If the T-stress of the main crack vanishes, the stability is governed by the g-term.

The following calculations focus on AS4 carbon warp-knit fabric composites, designed by The Boeing

Company, Long Beach for the all-composite wing skin in a commercial transport aircraft. Each layer of fabric with fiber volume content of 59.4% contains AS4 fibers, 44% in the 0° direction, 44% in the ±45° directions, and 12% in the 90° direction. Layers of fabric are stacked and stitched together to form the laminate. The resulting materials properties are:

$$E_X = 5.22\ Msi, \quad E_Y = 10.4\ Msi, \quad E_Z = 1.45\ Msi$$

$$G_{XY} = 2.54\ Msi, \quad G_{YZ} = 0.64\ Msi, \quad G_{XZ} = 0.57\ Msi$$

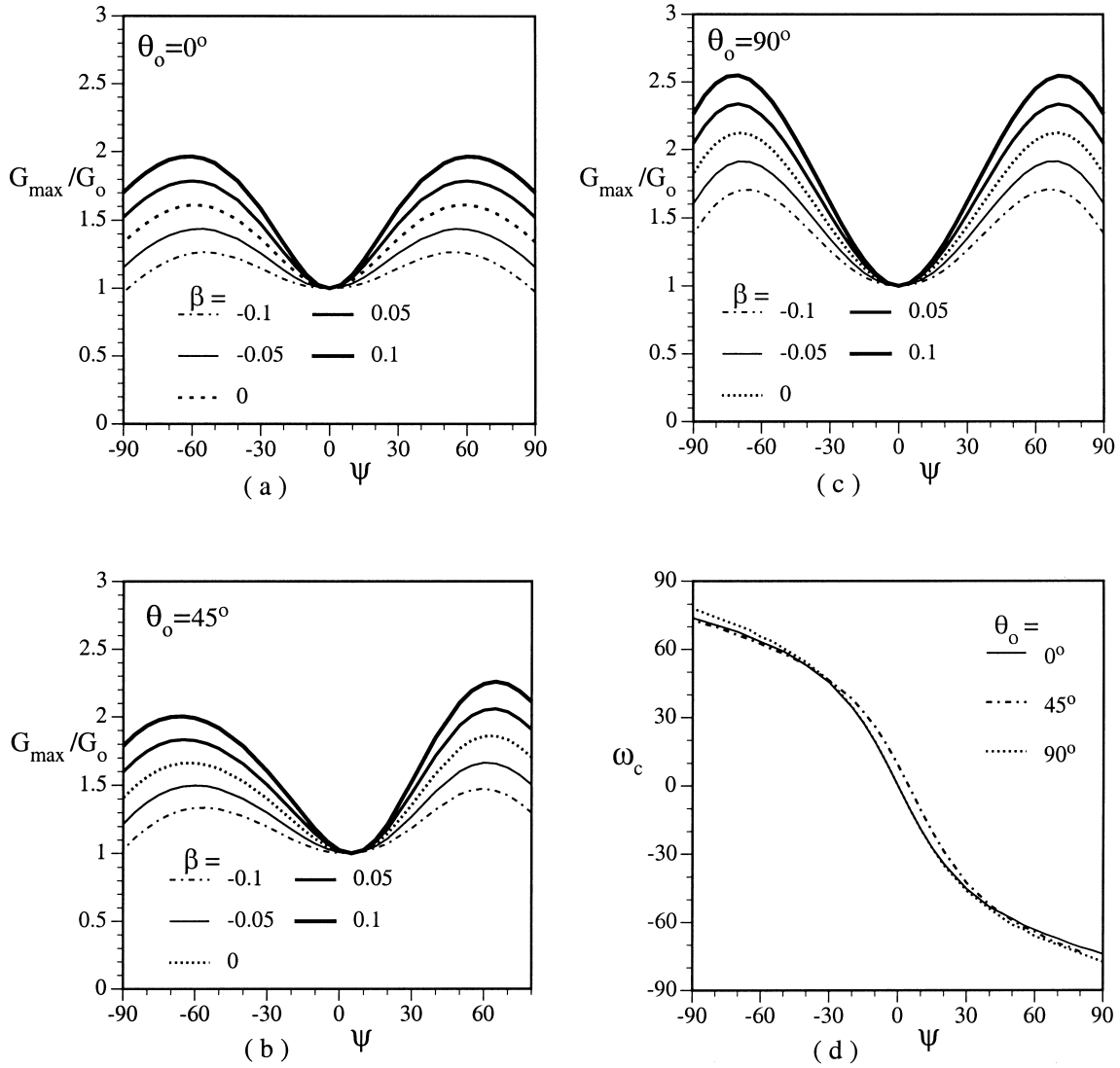

Fig. 11. Ratio $G_{\max}/G_0$ varies with the loading phase ψ for various values of the T-stress parameter β: (a) $\theta_0 = 0°$, (b)$\theta_0 = 45°$, (c)$\theta_0 = 90°$, (d) values of $\omega_c(\psi)$ at which the energy release rate $G(\omega)|_{T_1=0}$ reaches the maximum values.

$$\nu_{XY} = 0.202, \quad \nu_{XZ} = \nu_{YZ} = 0.49$$

The two nondimensional material parameters defined in Eq. (9.1) are

$$\lambda = 1.93, \qquad \rho = 1.18$$

In order to obtain the effects of crack orientation of the main crack in the composite, three orientations are chosen:

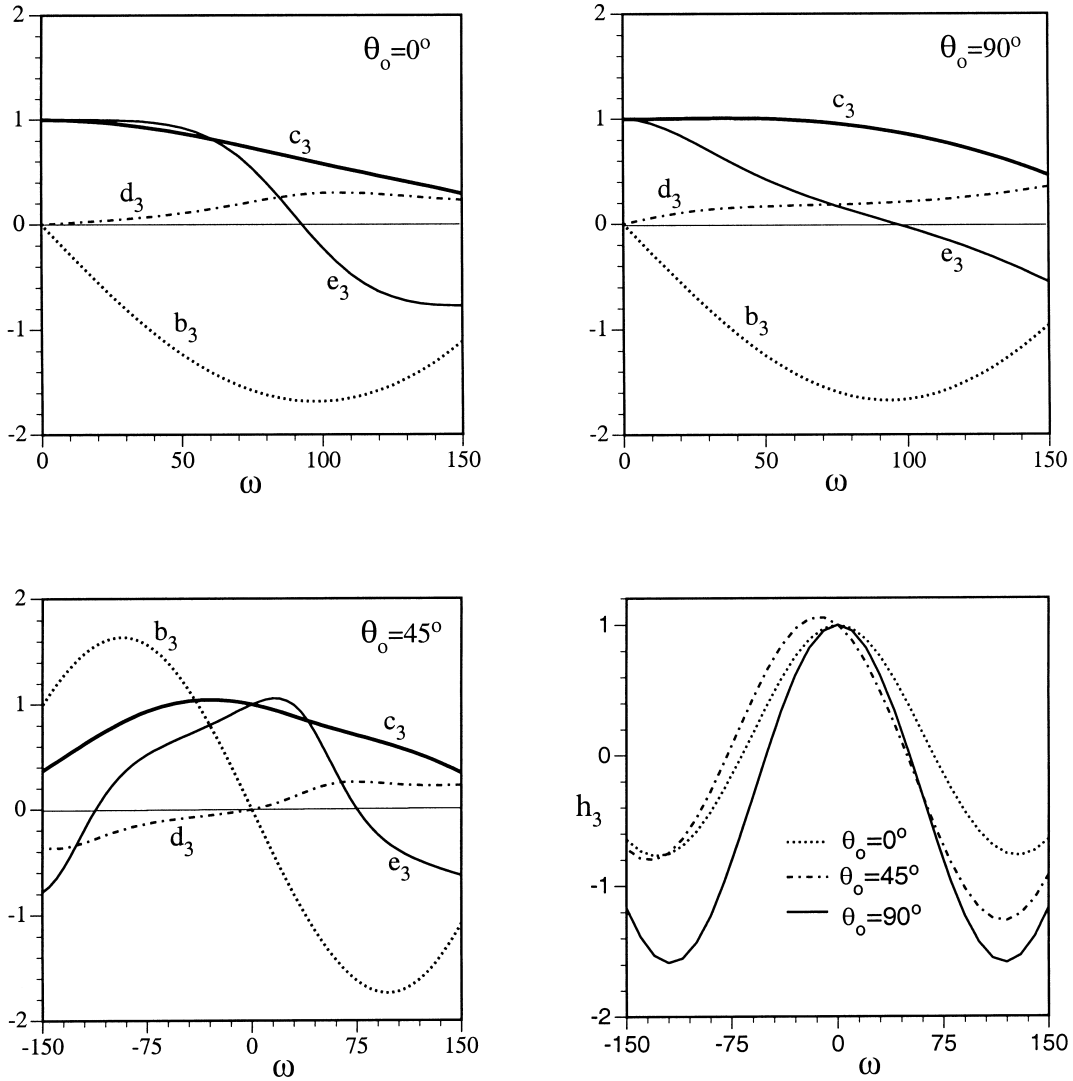

Fig. 12. Variation of coefficients c_3, b_3, h_3, d_3, and e_3 with the kink angle ω for three orientations of the main crack, $\theta_0 = 0°, 45°$, and 90°, in a composite with $s'_{yz}/s'_{xz} = 0.5$.

$\theta_0 = 0$, the main crack perpendicular to the stiffer material Y-axis
$\theta_0 = \pi/4$, the main crack inclined with 45° from the stiffer material Y-axis
$\theta_0 = \pi/2$, the main crack parallel to the stiffer material Y-axis;

The values of c_{ij}, b_i, h_{ij}, d_i, e, associated with in-plane deformation are presented in Figs. 5–7 for each orientation of the main crack. The detailed numerical values of these coefficients for selected kink angles are given by Tables 3–5. In Figs. 8–10, the ratios $G(\omega)/G_0$ are presented as functions of kink angle ω for various values of T-stress parameters, β, and loading mixity.

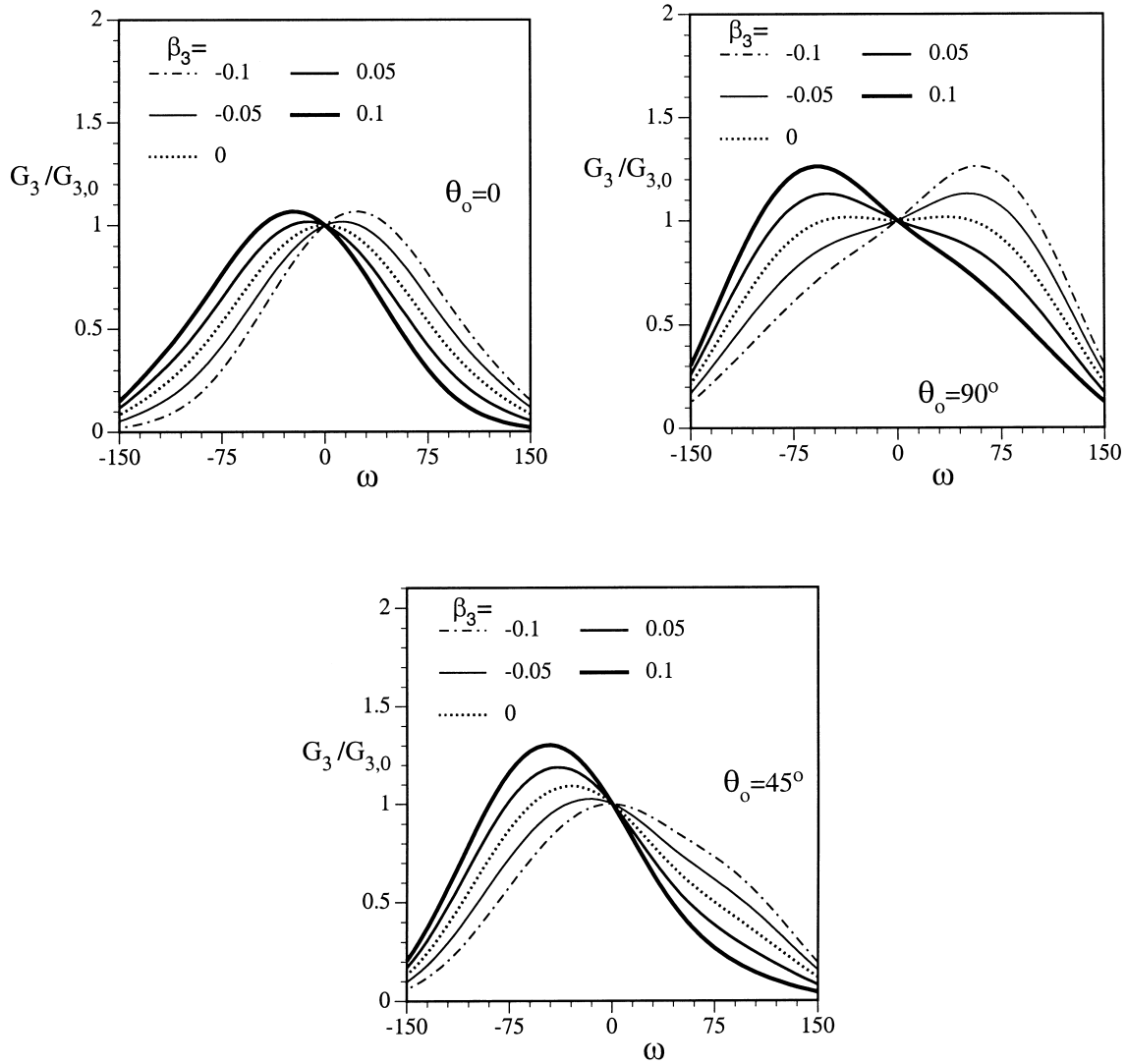

Fig. 13. Energy release rate ratio $G_3/G_{3,0}$ as a function of the kink angle ω for various values of the T-stress parameter β_3 for three main crack orientations, $\theta = 0°, 45°, 90°$, in a composite with $s'_{yz}/s'_{xz} = 0.5$.

Consider the case of $\theta_0 = 0^\circ$ shown in Fig. 8, for mode-I loading, G reaches maximum value for all β at $\omega = 0$. The positive T-stress increases the energy release rate and vice versa. The influence of T-stress on G increases with $|\omega|$. For example, G/G_0 at $\omega = 90^\circ$ increases 58% when β increases by 0.1. For $\psi = 5^\circ$, G attains a maximum value at $\omega = -6^\circ$, -9.9°, -17° for $\beta = -0.1, 0, 0.1$, respectively. The positive β increases G and shifts $G_{\max}$ to the negative direction of ω and vice versa. For $\psi = 45^\circ$, the effect of T-stress on G is very significant. The positive β increases G in most of the region where the kinked crack tip is open. Results show that the kinked crack tip is open in the range of $\omega < 30^\circ$. The

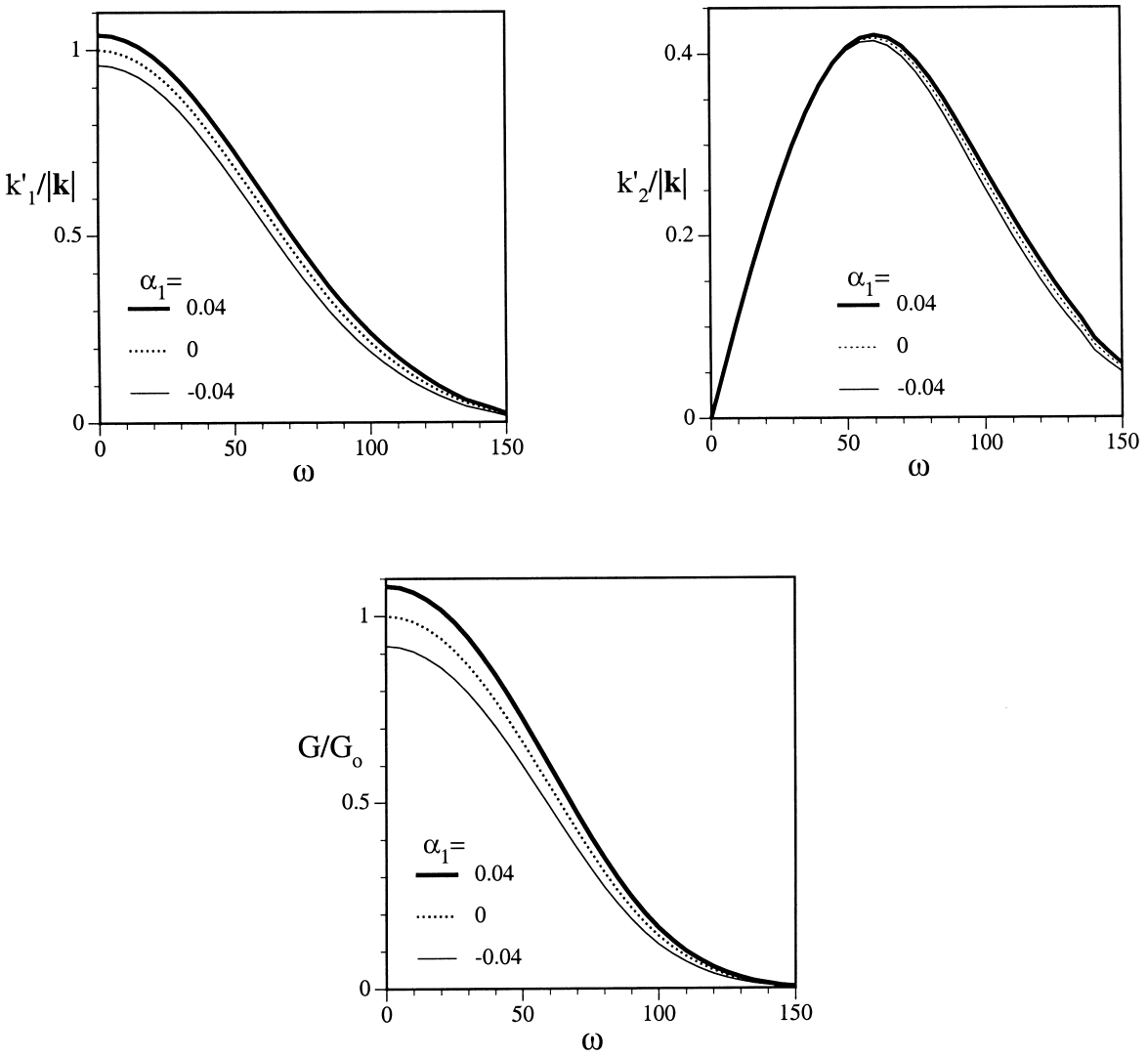

Fig. 14. Variation of the stress intensity factors k_1', k_2' and the energy release rate G at the kinked crack tip with kink angle ω for $T_1 = 0$ and $\theta_0 = 0^\circ$. The main crack is subjected to mode-I loading in a composite with $\lambda = 1.93$, $\rho = 1.18$.

values of G for the ranges of β studied has a maximum value around $\omega = -56.5^\circ$. When loading is pure mode-II, $\psi = 90^\circ$, the region where the kinked crack tip is open is $\omega < 0^\circ$. In the region around $\omega = -74^\circ$, G takes a maximum value.

In Fig. 9, when $\theta_0 = 45^\circ$, the main crack is open in the loading range $\psi < 80.75^\circ$. For the mode-I loading, $\psi = 0^\circ$, the kinked crack tip is open and $k_1' > 0$ in $\omega > -120^\circ$. The negative β reduces $G(\omega)$ in the open region and vice versa. The critical kink angles, ω_c, defined by the maximum energy release rate occur at $\omega_c = 0^\circ$, 9°, 20° for $\beta = -0.1, 0, 0.1$ (see Tables 6–10). Under mixed-mode loading, $\psi = 45^\circ$, the open region for kinked crack is $\omega < 40^\circ$ and the critical values for $G_{\max}$ are in the range $-56^\circ < \omega_c <$

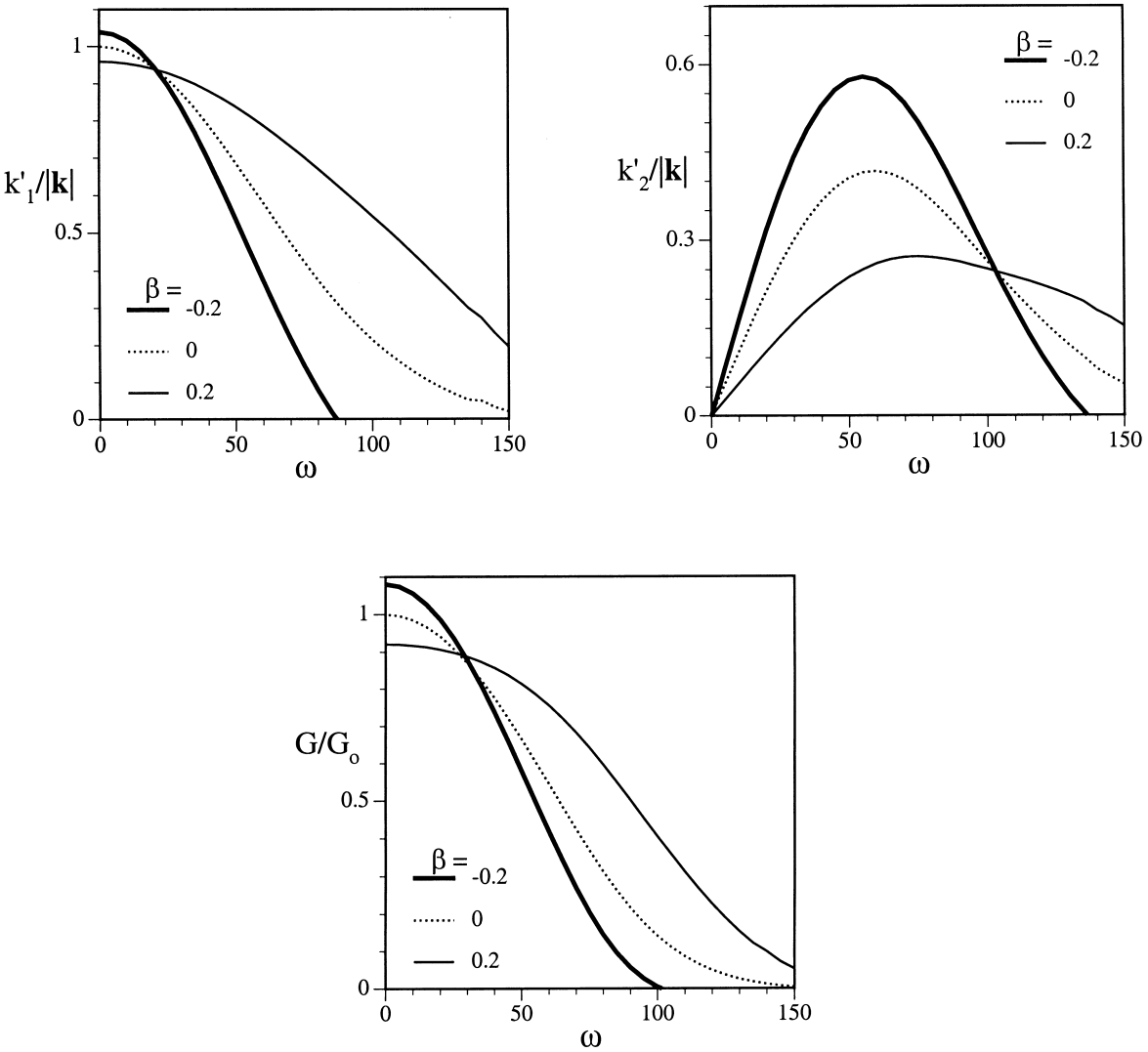

Fig. 15. Variation of the stress intensity factors k_1', k_2' and the energy release rate G at the kinked crack tip with kink angle ω for $\alpha_1 = -\beta|\beta|$ and $\theta_0 = 0^\circ$. The main crack is subjected to mode-I loading in a composite with $\lambda = 1.93$, $\rho = 1.18$.

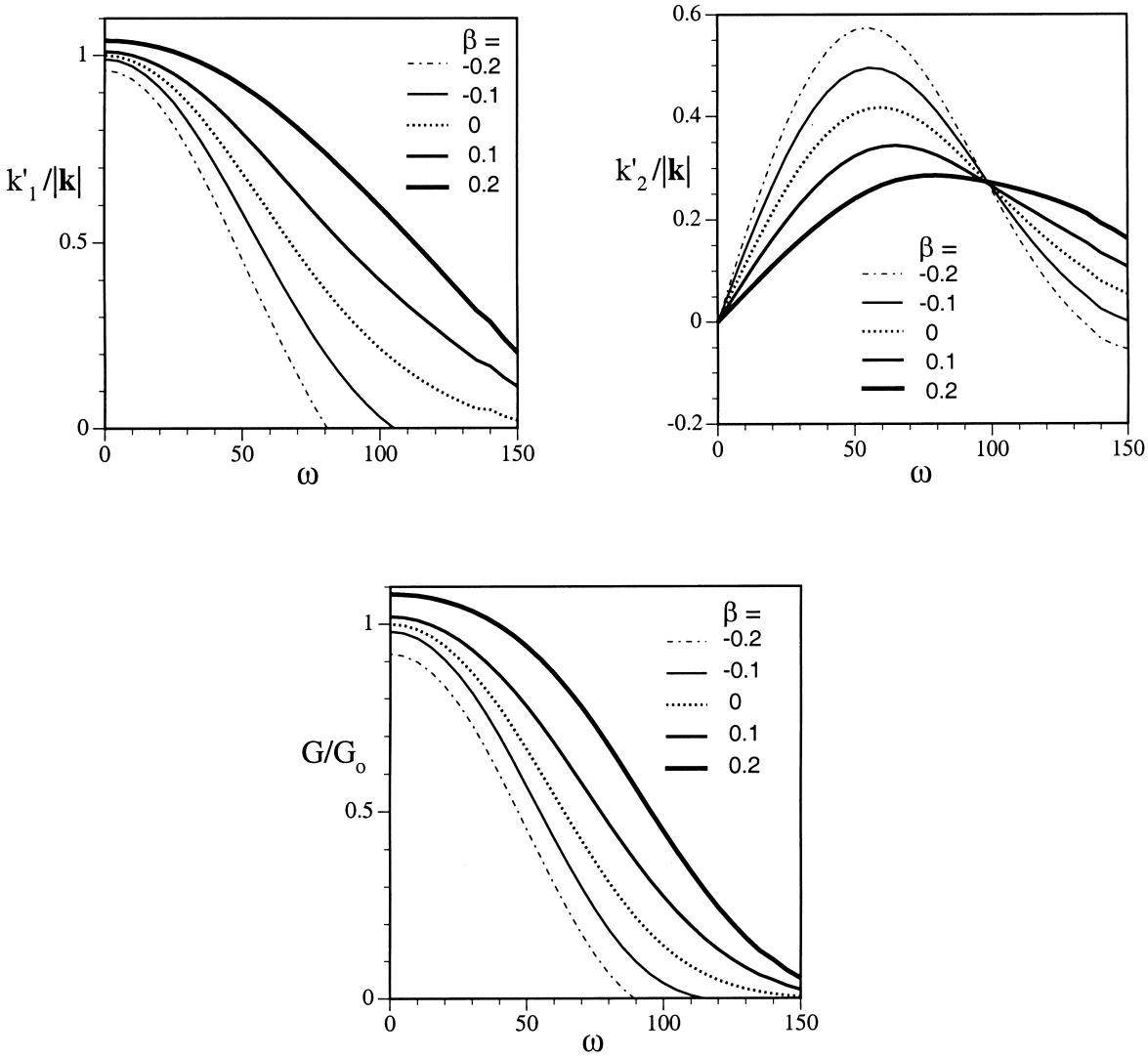

Fig. 16. Variation of the stress intensity factors k_1', k_2' and the energy release rate G at the kinked crack tip with kink angle ω for $\alpha_1 = \beta|\beta|$ and $\theta_0 = 0^\circ$. The main crack is subjected to mode-I loading in a composite with $\lambda = 1.93$, $\rho = 1.18$.

-45° for values of β studied. In Fig. 10, T-stress also plays very important role in crack kinking for the crack orientation, $\theta_0 = 90^\circ$.

Fig. 11 shows the maximum energy release rate for the entire loading phase with three crack orientations. The values of ω_c at which maximizes $G(\omega)$ for $\beta = 0$ are also shown in Fig. 11(d). Note that the value of $G_{\max}$ for $\beta \neq 0$ is in the neighborhood of ω_c. The actual $G_{\max}$ is higher than that given by the figure.

In the next set of Figs. 12 and 13, we consider the anti-plane deformation in an orthotropic material. Fig. 12 shows the variation of c_3, b_3, h_3, d_3, e_3 with kink angle for three main crack orientations in a composite with $s'_{YZ}/s'_{XZ} = G_{ZX}/G_{YZ} = 0.5$. The energy release rate $G_3(\omega)$ for different values of T-stress parameter, β_3, for the three crack orientations in the composite are illustrated in Fig. 13 which only

shows the first two terms in the expression $G_3(\omega)$ of Eq. (7.33). For crack orientation parallel to the material principal axes, the positive β_3 increases $G_{\max}$ and shifts the values to the negative values of ω and vice versa. For the unsymmetric crack orientation, $\theta_0 = 45^\circ$, the positive β_3 increases $G_{\max}$.

In the above Figs. 3–13, the terms with order a^0 and $\sqrt{a}$ on the kink behavior are discussed. The effect of higher-order terms with order a is shown from a set of Figs. 14–16. These figures show the variation of the stress intensity factors, k_1', k_2' and energy release rate G at the kinked crack tip with ω in the AS4 fabric composite. The main crack with orientations $\theta_0 = 0^\circ$ is subjected to mode-I loading. These figures represent three cases: $T_1 = 0$; $T_1 g_1 \leq 0$; $T_1 g_1 \geq 0$. They show the effects of higher-order terms for different combinations. These figures further provide information of the kink crack stability.

In summary, a kinking analysis for a crack in a generally anisotropic solid under two-dimensional deformation has been performed. Based on Stroh formalism and a singular integral equation method, the expressions of stress intensity factors, T-stress, energy release rate at the kinked tip in terms of k-term, T-term, and g-term acting on the main crack prior to kinking has been formulated and calculated. The effects of T-stress and the third term applied at the main crack field on the kinking and stability of the kinked crack are determined. The stability condition of the kinked crack has been developed based on the energy release rate fracture criterion. The influences of material anisotropy, crack orientation, and load mixity on the crack kinking behavior are discussed in detail through many numerical results.

Acknowledgements

The authors wish to acknowledge the financial support provided by NASA Grant No. 98- 0548 from NASA Langley Research Center under Advanced Composite Technology program.

References

Banichuk, N.V., 1970. Using the small-parameter method to determine the form of a curved crack. Izv. An SSR, MTT 5 (2), 130–137.

Bibly, B.A., Cardew, G.E., 1975. The crack with a kinked tip. International Journal of Fracture 11, 708–712.

Cotterell, B., Rice, J.R., 1980. Slightly curved or kinked cracks. International Journal of Fracture 16 (2), 155–169.

Erdogan, F., Gupta, G.D., 1972. On the numerical solution of singular integral equations. Quarterly Applied Mathematics 29 (3), 525–534.

Erdogan, F., Gupta, G.D., Cook, T.S., 1973. Numerical solution of singular integral equations. In: Sih, G.C. (Ed.), Methods of Analysis and Solutions of Crack Problems. Noordhoff, Leiden, The Netherlands, pp. 368–425.

Gao, H., Chiu, C.H., 1992. Slightly curved or kinked cracks in anisotropic elastic solids. International Journal of Solids and Structures 29 (8), 947–972.

Gol'dstein, R.V., Salganik, R.L., 1974. Brittle fracture of solids with arbitrary cracks. International Journal of Fracture Mechanics 10 (4), 507–523.

Hayashi, K., Nemat-Nasser, S., 1981. Energy-release rate and crack kinking under combined loading. ASME Journal of Applied Mechanics 48, 520–524.

He, M., Hutchinson, J.W., 1989. Kinking of a crack out of an interface. ASME Journal of Applied Mechanics 56, 270–278.

He, M., Bartlett, A., Evans, A.G., 1991. Kinking of a crack out of an interface: role of in-plane stress. Journal of American Ceramic Society 74 (4), 767–771.

Hutchinson, J. W., Suo, Z., 1992. Mixed mode cracking in layered materials. Advances in Applied Mechanics 29, 63–191.

Khrapkov, A.A., 1971. The first basic problem for a notch at the apex of an infinite wedge. International Journal of Fracture Mechanics 7 (4), 373–382.

Khrapkov, A.A., 1998. Riemann problem on imaginary axis and its application in fracture mechanics. In: Cherepanov, G.P. (Ed.), Chapter 8 Fracture: A Topical Encyclopedia of Current Knowledge. Krieger, Florida, pp. 125–195.

Lo, K.K., 1978. Analysis of branched cracks. ASME Journal of Applied Mechanics 45, 797–803.

Melin, S., 1994. Accurate data for stress intensity factors at infinitesimal kinks. ASME Journal of Applied Mechanics 61, 467–470.

Miller, G.R., Stock, W.L., 1989. Analysis of branched interface cracks between dissimilar anisotropic media. ASME Journal of Applied Mechanics 56, 844–849.

Muskhelishvili, N.I., 1953. Singular Integral Equations. P. Noordhoff, Groningen, Holland.

Obata, M., Nemat-Nasser, S., Goto, Y., 1989. Branched crack in anisotropic solids. ASME Journal of Applied Mechanics 56, 858–864.

Selvarathninam, A.S., 1995. A generalized linear elastic fracture mechanics model for advanced materials, Ph.D Thesis, Clemson University.

Suo, Z., Bao, G., Fan, B., Wang, T.C., 1991. Orthotropy rescaling and implications for fracture in composites. International Journal of Solids and Structures 28 (2), 235–248.

Sumi, Y., Nemat-Nasser, S., Keer, L.M., 1983. On crack branching and curving in a finite body. International Journal of Fracture 21, 67–79.

Ting, T.C.T., 1996. Anisotropic Elasticity, Theory and Applications. Oxford University Press, Oxford.

Wu, C.H., 1978. Fracture under combined loads by maximum-energy-release-rate criterion. ASME Journal of Applied Mechanics 45, 553–558.

Yang, S., Yuan F.G., 1999. Determination and representation of the stress coefficient terms by path-Independent integrals in anisotropic cracked solids, International Journal of Fracture, January, 1999, submitted.